Optimal Design and Testing of Laminated Specimens to Evaluate Competing Composite Failure Criteria

by

Arend Andries van Wamelen

Thesis submitted to the faculty of the
Virginia Polytechnic Institute and State University
in partial fulfillment of the requirements for the degree of

Master of Science

in

Aerospace Engineering

APPROVED:

Eric R. Johnson, Co-chairman

Raphael T. Haftka, Co-chairman

Zafer Gürdal

July, 1993

Blacksburg, Virginia

Optimal Design and Testing of Laminated Specimens to Evaluate Competing Composite Failure Criteria

Arend Andries van Wamelen

Eric R. Johnson and Raphael T. Haftka, Chairmen

Aerospace Engineering

(ABSTRACT)

Optimization methods are used to find areas of maximum disagreement between the failure criteria of Tsai and Hart-Smith. The Tsai criterion is quadratic in the stresses and employs a selective and progressive ply-by-ply degradation scheme to predict ultimate load. Hart-Smith's criterion is based on a fiber shear failure of the fibers and also predicts ultimate load. Both compression-compression and tension-shear combinations are identified as areas of large difference in predicted failure loads. Graphite-epoxy specimens are designed to maximize the difference in the failure loads computed from the two criteria under uniaxial tension. Both on-axis and ten-degree off-axis specimens are designed and tested. The laminates that maximize the difference in these criteria exploit the manner in which they treat the effect of in-plane shear on the failure prediction. Test results indicate little difference in the failure prediction for the on-axis test. However, the off-axis tests show that the Tsai criterion predicts failure much closer to the test results.

Acknowledgements

This work was partially funded through NASA grant NAG-1-168.

I wish to thank Mr. David Beck of BASF Structural Materials, Inc. for providing the material used for the experiments, Dr. Stephen W. Tsai for providing the computer code used to check our coding of his failure criterion, Dr. John Hart-Smith for discussions on his failure criterion during a visit to Virginia Tech, for providing a set of his recent papers on failure prediction, and for his suggestions concerning our results. Mr. Jack Lesko was very helpful with suggestions and practical advice on testing, specimen preparation, and yacht racing.

In particular I would like to thank my co-chairmen, Dr. Raphael Haftka and Dr. Eric Johnson for making this work possible. Dr. Haftka provided the idea the study was based on, arranged the all-important assistantship, and supplied advice on optimization and other aspects. Dr. Johnson provided many hours of patient discussion on all aspects of the work, and was instrumental in guiding the work. Dr. Zafer Gürdal is thanked for agreeing to serve on my committee on short notice.

Finally, I would like to thank all my friends in Blacksburg for making the years here worthwhile on the personal level.

Table of Contents

List of Figures

List of Tables

Chapter 1 : Introduction

1.1 Background

It is common in the fields of engineering and the physical sciences to make extensive use of experimental data for predicting the response of physical phenomena. Sometimes purely empirical models are obtained by interpolating experimental data. More commonly, models of physical phenomena are derived analytically, but these models are either verified by experiment or have had their theoretical assumptions validated by experiment. When different models of the same phenomenon exist, experimental data is very persuasive in showing relative merit. A whole discipline, called system identification, has grown from the practice of improving analytical models based on experimental results.

Clearly, the use of experiment in model building, verification, comparison of models and acquiring basic properties is well established. Different uses for experimental data exist but as experiments are typically very expensive and time consuming, it is in all cases of considerable concern that the least number of tests produces the most significant data. Optimization techniques are often used in design and analysis of systems, but are also useful in the test and design process.

One field for which competing models of the same phenomenon abound is failure prediction for composite materials. In one survey, [1, pp. 71-125], 22 criteria are described. Unlike for metals, no failure theory has been generally accepted. Composite materials display many different failure modes, including fiber, matrix and interface failures, making prediction difficult. Even for simple in-plane loading under plane stress conditions, a generally accepted theory is lacking. The issue of comparing and evaluating the relative merit of these criteria now arises. In this study the differences between two composite failure criteria are accentuated by using optimization methods to find areas of greatest disagreement. Experiments are then conducted in one of these areas to find which model performs best.

1.2 Optimization and experiments

Multiple connections between optimization and experiments occur at various stages of analysis and design. These stages include model building, design optimization, design validation, system identification, and quality control. In summary, the discussions given by Haftka [2] on these stages are:

- In model building optimization can be used to a) reduce the number of experiments needed to verify the model, b) reduce the number of experiments needed to find constants associated with the model, and c), design experiments that will discriminate between competing models and improve their accuracy.
- Experimental results can be used directly to design optimal systems in cases where models are either unavailable, inaccurate, or too expensive to use.
- System identification employs optimization to determine model constants that best match experimental results.

- In quality control, optimization can be used to design a sampling system for optimizing the reliability required of a product.

A field known as parameter estimation [3] exists, and in its simpest form is concerned with finding the parameters associated with a model of a phenomenon observed. This process is similar to system identification. In parameter estimation the model is already known, but certain parameters are needed to fit the model to the observations. Part of parameter estimation is the problem of design of experiments. Here the known experimental conditions are optimized, so as to maximize the sensitivity of unknown parameters that are to be estimated.

Of many connections between optimization and experiments itemized above, experimental design for maximum sensitivity to unknown parameters and discriminating between competing models are the most germane to the present study.

1.2.1 Sharpening the differences between competing models

Typical ways of designing experiments to validate theory include arbitrary selection of test cases or use of standard tests. For example, the use of standard tests is common in the field of finite element development. As discussed by Haftka and Kao [4], some of these traditional approaches to verifying new models may be inherently flawed. In the case of arbitrary selection of test cases it is suggested that a form of "natural selection" can conspire against researchers. Different researchers may independently try an idea for a new model. If the model is not good most investigators will conclude this from their experiments. It is possible though, that one person will pick test conditions where the model coincidentally agrees with experiment. Only this researcher is likely to publish the results, leading others to believe the model has general validity.

The practice of using standard tests can also be flawed. For the common case of standard tests being used to check new models it is suggested [4] that primarily models doing well for the specific test cases will be selected, as opposed to those with general validity. The idea of using test cases is of course to test general validity, but this may only be possible when a large number of standard tests are required.

Instead of using arbitrary experiments or standard test cases, Haftka and Kao suggest that new models should be compared to old ones to find areas of greatest disagreement. The

search for such areas could be done either analytically or by using optimization techniques. Performing a test in the area of greatest disagreement is most likely to provide a challenging test. As an example, Haftka and Kao maximized the difference between two finite element models of beam deflections by varying the load distribution on the beam. One model used Bernoulli-Euler beam elements while the other used plane-stress elements. The optimization problem was to find the load distribution causing the greatest difference in strain energy for the two models. A load distribution exploiting the fact that the Bernoulli-Euler solution ignores shear deformation was found by the optimizer, correctly identifying the weakness of this model.

Optimization can be used to find test conditions that accentuate the difference between two competing models of the same phenomenon. Haftka and Kao's illustration for this use of optimization involve two composite material failure criteria, the first-ply failure criteria of Tsai-Hill and Tsai-Wu. First, the set of in-plane stresses that result in the largest ratio of failure indices was found, with the stresses treated as independent design variables in the optimization. Then a model of a plate with a hole was considered. Here four geometric and load design variables were varied to find the largest difference in failure indices. For the laminate containing a hole, the stress components are of course not individually variable but change as result of chages in the design variables. Even so, a failure index ratio close to the theoretical maximum (laminate without a hole) was found. However, it is noted by Haftka and Kao that the critical ply changes as a function of the design variables, leading to a non-smooth optimization problem.

The case being studied here is similar in concept to maximizing the difference between the Tsai-Hill citerion and the Tsai-Wu criterion discussed above. But this study differs in some important details and in its scope with respect to the example given by Haftka and Kao, as is enumerated in the following section.

1.3 Objectives and approach

The objectives of this study are twofold.

- First, the study will focus on the use of optimization techniques to design experiments that differentiate between competing models of the same phenomenon.

- Second, this idea will be applied to failure criteria for filamentary composite materials with the objective of examining their relative merit when compared to experiment.

The failure criteria compared are those of Tsai and of Hart-Smith. Explanation of this choice is given later. The approach used is to first select suitable types of tests that can be performed in the Virginia Tech Aerostructures Axial-Torsional Test Facility, and then design optimal specimens that yield the greatest difference in predicted failure load. A series of experiments using the optimal specimens are conducted, and the actual failure loads are compared to predictions. It is hoped that this will provide insight into both the experiment design process and the relative merit of the two failure criteria under consideration.

The specific criterion proposed by Tsai [5, ch. 8, 9] considered here includes final ply failure employing an iterative ply degradation scheme. Hart-Smith's criterion [6, 7] is based on fiber failure in shear, and is represented by a hexagonal envelope in strain space. For the Hart-Smith failure criterion, the failure envelope is not a simple analytic function of the stress components. As a result, an analytic solution of the optimization problem is not feasible. Design variables include the applied load ratio and the laminate stacking sequence.

1.4 Organization of the report

In this chapter the topic of using optimization in the design of experiments was introduced. The following chapter focuses more closely on composite material failure prediction, and in particular provides all the information needed to implement the criteria of Tsai and Hart-Smith. The subjects of Chapter three are the test design, related optimization problems, and the examination of different solutions. Chapter four is concerned with the experimental process itself and gives information on manufacturing of test specimens, equipment used and the test procedures. Test results are presented in Chapter five, including comparison with prediction and discussion of the meaning of what was found. Future work is also discussed in Chapter five. Finally the work is rounded off with a short summary of the work, and a conclusions section.

Chapter 2 : Failure Criteria

2.1 Introduction

Failure prediction in composite materials is an area of great importance. Knowing how to accurately predict failure leads to the opportunity of using a material safely and to its full potential. Typically one needs to be able to assess the strength of a structure with complex geometry, different lamination sequences, and different load cases. For composite materials however, failure prediction is not simple, even at the lamina level. Orthotropy and a non-homogeneous microstructure complicates matters greatly.

Considering a filamentary composite material at the lamina level, it is obvious that at least three modes of failure may be possible. Either the fibers, matrix, or the fiber-matrix inter-

face can fail. In addition, the failure mode for tension and compression loading can be different for both the fiber and matrix. Available strength data would typically be based on uniaxial load tests, but these tests would mainly trigger a single mode of failure. In practice, however, the lamina is likely to be loaded at least biaxially. As a result one has to predict how the lamina would respond to states of combined loading. For materials orthotropic in strength and stiffness, a simple rotation of stresses to principal axes, as is a common first step for isotropic materials, is no longer helpful. Everything depends on the orientation of the loads and properties with respect to the fiber direction. The failure criterion now needs to predict how the different elements of loading will interact to cause failure. The use of uniaxial data for predicting the strength in biaxial loading cases is the central problem in composite failure criteria.

At the laminate level additional difficulties arise. It is possible to use classical lamination theory to find the stresses in each lamina and simply apply a lamina failure criterion ply by ply. The effect of lamination, however is then ignored. It is well known, for example, that failure of one ply does not necessarily lead to catastrophic failure of the laminate. In this case some form of progressive damage model, or a model that directly predicts total failure is needed. Stacking sequence is also known to have an effect on laminate strength. For example, laminates with too many contiguous plies of the same orientation often crack in the matrix, even under thermal stresses during cool-down alone. Interlaminar failure, or delamination, is also a common and insidious mode of failure initiation in many laminated structural components.

For these reasons a fully analytic failure criterion, integrating the different failure modes into a rational prediction methodology has yet to be developed. There is no dearth of attempts at failure criteria, though, with some references describing 22 distinct proposals [1, pp. 71-125]. Most criteria treat the material to some extent as a homogeneous orthotropic body. Empirical means of interpolating uniaxial data for biaxial cases are common.

Simply checking each of the stresses in fiber coordinates against the stress at failure in the uniaxial test is the simplest form of composite strength prediction. This is the well known maximum stress criterion [8, pp. 72-74]. As interaction of failure modes is entirely ignored, this method is of little value, beyond quick qualitative inspection of stress levels. Checking each strain component in a similar way is known as the maximum strain criterion. It is also known to be inaccurate [8, pp. 74-76], yet it is widely used, with appropri-

ately large safety factors, in the aerospace industry. This is less of a compliment for the criterion than a measure of how little industry believes the more complex criteria. According to Hart-Smith [9], this criterion is accurate in the tension-tension and compression-compression quadrants, but known to be unconservative in the other two. Nevertheless, he refers to it as "until now.... the best failure model available for fibrous composites".

Some of the earliest attempts at failure prediction for anisotropic materials were made to characterize wood [1, p. 75]. In 1950 Hill generalized the distortion energy yield criterion of von Mises for anisotropic materials [8, pp. 76-80], [1, pp. 89-90]. Hill's work was on the anisotropy in rolled metals, where the properties become directional with respect to the rolling axis. Three important differences with composites should be noted: first, the degree of anisotropy is fairly small, second, the rolled material remains homogeneous, and finally, the model was developed to predict yield while most composites fail in a brittle fashion with little or no yielding. Even so, Tsai and Azzi adopted Hill's criterion for use with composite materials [10]. This "Tsai-Hill" criterion accounts only for equal tensile and compressive strengths, but was adapted by Hoffman[11] in 1967 to accommodate unequal strengths.

In an attempt to achieve better prediction by allowing more terms in the prediction equation some authors introduced the use of strength tensors. One of the first proposals using strength tensors was by Gol'denblat and Kopnov [12]. Tsai and Wu published a tensor theory in 1971 [13]. The theory can be recognized as a simplification of the more general Gol'denblat and Kopnov work with the highest rank stress tensor now being 4th order as opposed to the Gol'denblat and Kopnov 6th order one. Known as the Tsai-Wu theory, it uses the usual five strength terms and in addition, a term related to the extent of interaction between failure modes. Ideally this term should be obtainable from biaxial tests, but as these tests are quite hard to do properly, the term is more commonly empirically determined.

During the late eighties, Tsai has been extending the Tsai-Wu criterion to include progressive evaluation of failure, introducing first- and last-ply predictions, [5, ch. 9], [14, ch. 11]. Some lesser known work by Puppo and Evenson and Wu and Scheulein proposed direct laminate strength theories [1, p. 75]. Recently Hart-Smith proposed a criterion intended purely to predict fiber failures in laminates [6], [7], and [15]. Hart-Smith argues that none of the criteria to date are truly able to include distinct failure modes. He limits the use of

his criterion to fiber dominated laminates, defined as laminates that are so dominated by fiber strength that matrix effects are unimportant, arguing that matrix-dominated laminates are by definition bad, removing the desire to quantify their strength.

The list of criteria mentioned above is by no means exhaustive, but includes the popular ones and is intended to highlight the different approaches to failure prediction.

Among the criteria offered, the Tsai-Wu theory is the most widely taught one, and is included in several finite-element codes. Various versions including degradation are available in composite analysis codes [5, Appendix B]. The latest version, [5, ch. 9], includes complete ply-by ply failure sequences.

The criterion of Hart-Smith has recently begun to attract considerable attention, among other things for its physical basis. Hart-Smith is quite outspoken in his papers on the unsuitability of "curve-fit" type criteria, (his characterization of tensorial criteria), criticizing them for not being grounded in physical arguments and therefore being unscientific.

For the sake of this investigation into experiment design, the criteria of Hart-Smith and Tsai (including progressive failure) have been selected for comparison. The criteria are very current, with new material on both criteria having been published as recently as 1992. The methods of analysis of failure are also completely different, creating the prospect of a non-trivial optimization problem.

The following two sections are devoted to explaining the basis and application of the two criteria.

2.2 Strain-based maximum shear stress failure criterion of Hart-Smith

Hart-Smith's criterion is based on the well known Tresca maximum shear stress yield criterion for ductile isotropic homogeneous metals. This criterion is first expressed in strain form and then interpreted for composite materials. Tresca's criterion is based on failure by a shear mechanism, and Hart-Smith presents evidence that some typical reinforcements, like carbon fibers, fail by the same mechanism [7]. The central idea separating this criterion from most previous composite failure criteria is that separate failures are allowed for the matrix, fiber, and fiber-matrix interface. To date the theory only accounts for fiber fail-

ures. According to Hart-Smith, failure of the different constituents should be treated separately, and their contributions superimposed in strain space to find the lamina or laminate criterion. The empirical means by which Tsai and others draw smooth curves through the failure points of the different constituents is rejected as unscientific.

Hart-Smith states that a truly general failure criterion should be a two-phase theory, with different criteria for each constituent superimposed. As only the fiber criterion is available to date, certain limitations must be placed on laminates to be analyzed by this criterion. Only fiber dominated laminates are to be considered. These are defined as laminates for which structurally significant failures of the matrix does not precede fiber failure. Hart-Smith reasons that this is not too strict a limitation, as laminates that fail in the matrix are by definition bad, removing the desire to predict their strength. In addition he states that a similar restriction should apply to the traditional homogenized theories, as they too are incapable of differentiating between good and bad laminates. To quote Hart-Smith [7]:

> *It does not seem realistic to delay the application of the most realistic failure model for conventional fibrous composites merely because the theory is valid only for structurally efficient laminates and, like all the theories that preceded it, cannot of itself identify structurally inefficient fiber patterns.*

In order to ensure fiber dominated laminates, at least 12.5% of fibers in each of the 0°, 90°, 45°, and –45°, directions are required. In addition, it is recommended that the number of plies in each set of perpendicular directions be similar; i.e., as many +45° plies as –45° plies, etc.

2.2.1 Tresca failure criterion

The Tresca criterion, or maximum shear-stress criterion, assumes that yielding for isotropic homogeneous materials occurs whenever the maximum shear stress reaches the value it has when yielding occurs in a tensile test. The maximum shear stress is one-half the difference between the maximum and minimum principal stresses, and it occurs on faces inclined at 45° to the faces on which the maximum and minimum principal stresses act. In the tensile test the maximum shear stress is $\frac{\sigma_0}{2}$, where σ_0 is the normal stress at yield. Thus, the Tresca criterion states that yielding occurs when

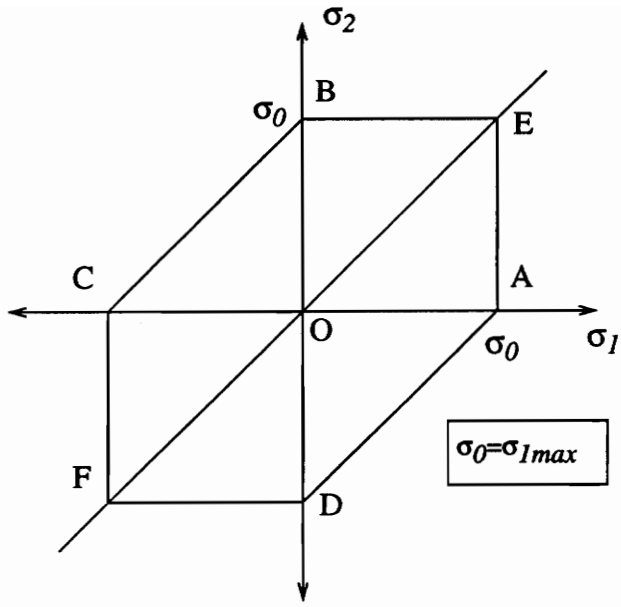

Fig. 2.1 Tresca criterion in stress space for an isotropic material; σ_3=0.

$$\tau_{max} = Max\{\left|\frac{\sigma_i - \sigma_j}{2}\right|\} = \frac{\sigma_0}{2} \qquad i,j = 1, 2, 3 \tag{2.1}$$

in which σ_i or σ_j denotes one of three the principal stresses at a point.

In the principal stress space (σ_1, σ_2, σ_3) the Tresca criterion is represented as a hexagonal cylinder with the cylinder's axis coincident with the ray through the origin and passing through coordinate (1,1,1); i. e., the ray in principal stress space associated with the hydrostatic state of stress. The intersection of this hexagonal cylinder with the σ_1-σ_2 plane (σ_3 = 0) is shown in Fig. 2.1. In this figure the 45° lines are associated with yield in the 1-2 plane, while the vertical and horizontal lines correspond to maximum shear stresses occurring in the 1-3 and 2-3 planes, respectively.

The criterion can also be expressed in terms of critical shear *strain*, or equivalently, a critical *normal strain difference*. To find this strain difference, consider the state of uniaxial tensile stress represented by point A in Fig. 2.1. From Hooke's law for the stress at point A, $\varepsilon_1 = \varepsilon_0 = \frac{\sigma_{1max}}{E}$, and $\varepsilon_2 = -\nu\,\varepsilon_0$, in which E is the modulus of elasticity and ν is

Poisson's ratio. The critical strain difference is $\varepsilon_1 - \varepsilon_2 = (1+\nu)\,\varepsilon_0$. Using this critical strain difference Fig. 2.2 can be drawn. The points labeled A, B, ..., F in Fig. 2.2 are the

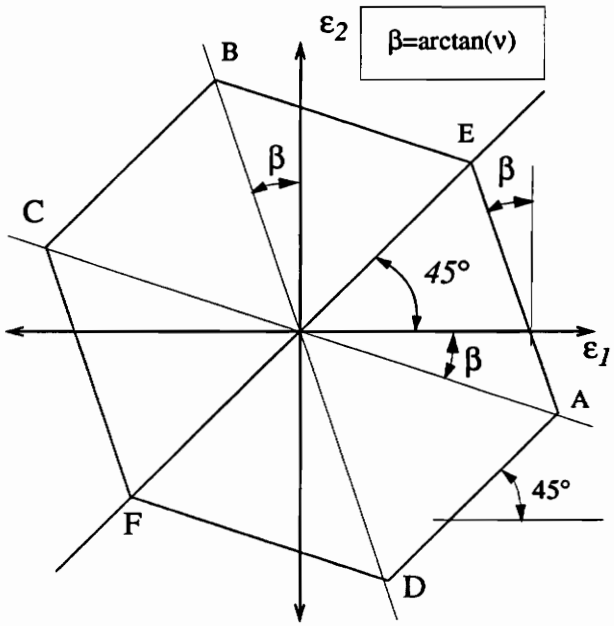

Fig. 2.2 Tresca criterion in strain space for an isotropic material.

strain states corresponding the similarly labeled stress states in Fig. 2.1. For isotropic materials the directions of principal stress and strain coincide, so the axes in Fig. 2.2 correspond to principal strains. (Note that $\varepsilon_3 \neq 0$, since in plane stress $\varepsilon_3 = -\nu\,(\sigma_1 + \sigma_2)/E$.) Points A and C correspond to pure tensile and compressive stress states in the *1*-direction, respectively, while points B and D are correspond to similar states of stress in the *2*-direction. These points do not lie on the principal strain axes due to the effect of the material Poisson's ratio. To derive the slope of line A-E and C-F consider loading the material transversely from point A, the point of maximum longitudinal stress. At this point the critical difference is generated simultaneously in the *1-2* and *1-3* planes. When the axial stress is held constant and the transverse stress is increased, the *1-2* plane ceases to be critical but the *1-3* plane remains critical. At point E the *1-3* and *2-3* planes become simultaneously critical. The slope of the lines is defined by the Poisson's ratio, as shown in the figure. The same argument can be used to find lines C-F. Note that the figure is doubly symmetric

about the lines at 45° with the axes. This symmetry is due to the isotropy of the material, with only one Poisson's ratio being present. For the new theory this symmetry is lost.

As was mentioned, this theory was proposed to predict yielding for ductile isotropic materials and applied using the principal stresses. None of these conditions hold for fiber reinforced composites. The theory has however been reinterpreted by Hart-Smith in such a way that the traditional case becomes a special case of a new more general theory.

2.2.2 Hart-Smith interpretation of Tresca's criterion

Hart-Smith reinterprets Tresca's criterion for fiber failures in composite laminates. The failure envelope is drawn for a *single fiber* in strain space, but a simplifying assumption is made later so as to use the same figure for a unidirectional lamina. To justify the use of a shear based failure mechanism Hart-Smith refers to work at McDonnell Douglas [7], and to work by Drzal [16] which show scanning electron micrographs of failed carbon and boron fibers with characteristic 45° shear-failure surfaces.

When referring to fiber strains the axes are labeled L, T, and N for longitudinal, transverse and normal, respectively. It is assumed the fiber is transversely isotropic in the T-N plane, and that plane stress conditions exist ($\sigma_N = \sigma_{NL} = \sigma_{NT} = 0$).

The complete failure envelope is shown in Fig. 2.3, with each labeled vertex point corresponding to a similar point in the isotropic case (Fig. 2.2). The whole figure is generated from a single failure strain, as was the case for isotropic materials; once again the single mechanism of shear failure is assumed. Uniaxial fiber failure is used to find the critical strain differential, which in turn is used throughout the figure. Consider an uniaxial load in the fiber direction, with failure occurring at stress σ_{Lmax}. At this point the strain in the longitudinal direction will be $\varepsilon_L = \varepsilon_0 = \frac{\sigma_{Lmax}}{E_L}$, and the strains in the T and N directions both $-\nu_{LT}\,\varepsilon_L$, since the fiber is transversely isotropic, ($\nu_{LT} = \nu_{LN}$). In these expressions E_L is the longitudinal modulus of elasticity, and ν_{LT} is the major, or longitudinal, Poisson's ratio. The critical strain differential in both the L-T and L-N planes will accordingly be $\varepsilon_0\,(1 + \nu_{LT})$. This *strain differential*, based on uniaxial tension failure of a fiber, is used to define the entire envelope. It is referred to as γ_{crit} [6,7], and defined as

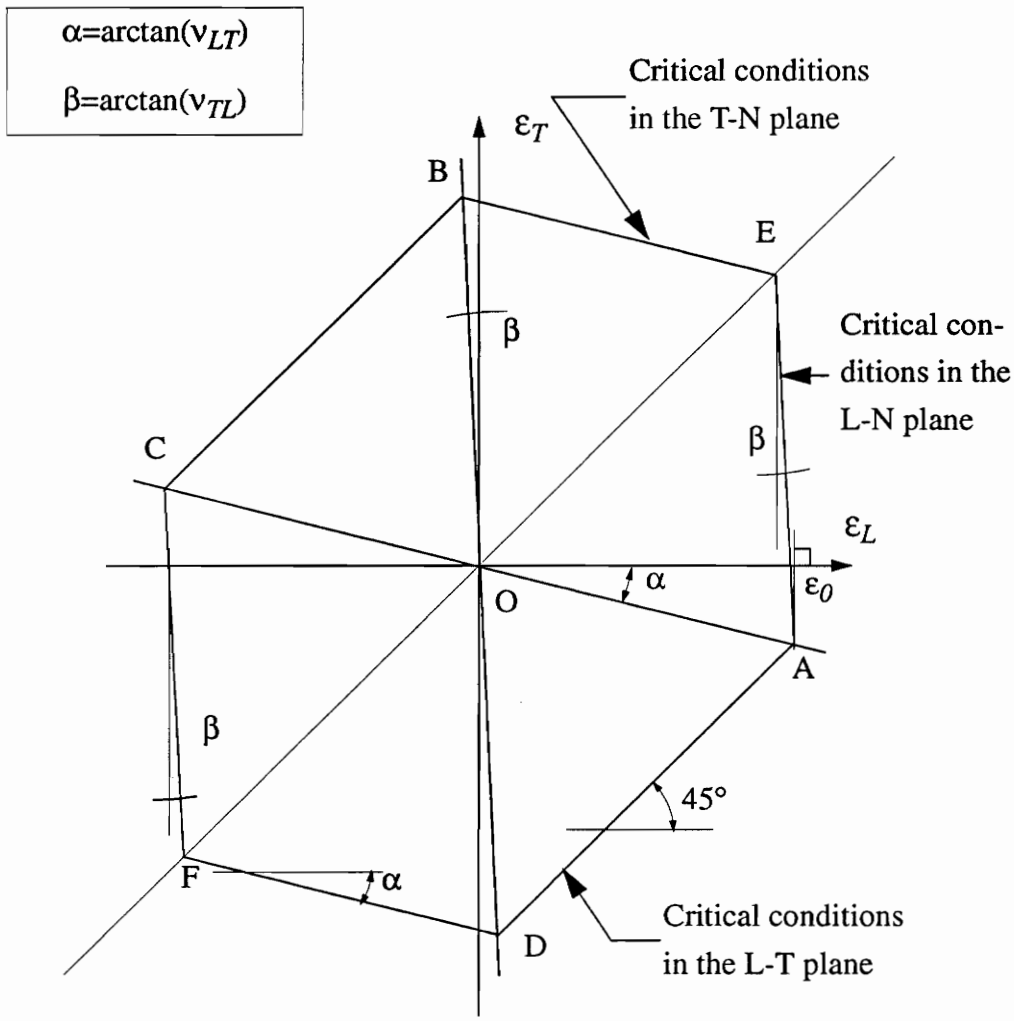

Fig. 2.3 Hart-Smith strain-based maximum shear stress failure criterion for a transversely isotropic fiber.

$$\gamma_{crit} = \varepsilon_0 (1 + \nu_{LT}) \qquad 2.2$$

The points A and C once again represent uniaxial loading in the L-direction. Poisson's ratio ν_{LT} defines the slope of line AC. The lines A-D and B-C are at 45° to the L-T axes through the uniaxial points A and C and represent the critical, and constant, ε_L-$\varepsilon_T = \gamma_{crit}$ difference in the L-T plane. It must be stressed that this strain difference does not imply a constant stress difference, unlike for the isotropic case. The material is not isotropic and has different E_L and E_T values, with E_T the modulus of elasticity in the transverse direc-

tion. Here it becomes clear that for transversely isotropic fibers, strain based definition of the criterion as proposed by Hart-Smith, is no longer analogous to a stress-based definition, unlike for isotropic materials.

The fiber transverse failure points, B and D, are found from an imaginary pure transverse load case ($\sigma_L = 0$, $\sigma_T \neq 0$, $\sigma_{TL} = 0$) for which the ratio of ε_L and ε_T strains is $-\nu_{TL}$, with ν_{TL} denoting the minor Poisson's ratio. The intersection of the pure transverse loading lines (O-B, O-D) with the 45° constant $\varepsilon_L - \varepsilon_T$ lines are *defined* as transverse fiber failure points. Note that the measured fiber *longitudinal* strain to failure is used here to indirectly define the *transverse* fiber strain to failure, based on the Poisson's ratios and stiffnesses.

As in Tresca's criterion, extension of the 45° lines beyond the pure longitudinal and transverse load points is not permitted as the strain differentials in the L-N or T-N planes then become too great, although the L-T differentials remain acceptable. To see how lines A-E and C-F are found, consider the fiber at point A. As in the isotropic case the L-N and L-T strain differences are both critical, and are given by $\gamma_{crit} = (1 + \nu_{LT})\varepsilon_0$. As in the isotropic case the L direction normal stress σ_L is held constant while the transverse normal stress σ_T is increased. The strains are now given by

$$\varepsilon_L = \varepsilon_0 - \frac{\nu_{TL}\sigma_T}{E_T} \qquad 2.3$$

$$\varepsilon_T = -\nu_{LT}\varepsilon_0 + \frac{\sigma_T}{E_T} \qquad 2.4$$

$$\varepsilon_N = -\nu_{LT}\varepsilon_0 - \frac{\nu_{TN}\sigma_T}{E_T} \qquad 2.5$$

in which ν_{TN} is the Poisson's ratio $-\varepsilon_N/\varepsilon_T$ for pure transverse loading. It should be clear that the ε_L-ε_T difference is reduced as expected, but that the already critical ε_L-ε_N difference, given by

$$\varepsilon_L - \varepsilon_N = (1 + \nu_{LT})\,\varepsilon_0 + (\nu_{TN} - \nu_{TL})\,\frac{\sigma_T}{E_T} \qquad 2.6$$

is increased, since ν_{TN} is larger than ν_{TL}. This was not the case for the isotropic material where all Poisson's ratios are the same. As a result it would seem that it is necessary for σ_L

to decrease as σ_T increases since $\nu_{TN} > \nu_{TL}$. Hart-Smith reasons that since this effect is caused by shear strains produced by *stresses out of the plane* of the shears under consideration, this is not reasonable. Shear strains to be considered when testing for failure are now *defined* to be all shear strains caused by *stresses in the plane* of the shear strain. For this interpretation the contribution of σ_T to the ε_L - ε_N strain differential, $(\nu_{TN} - \nu_{TL})\frac{\sigma_T}{E_T}$ in Eq. 2.6, is neglected, resulting in ε_L-ε_N remaining constant when σ_T is increased for fixed σ_L. This new general definition of the critical stain differential has no effect on the 45° lines as the only stresses are in the plane of critical strain difference, plane L-T. Line C-F is found in similar fashion to A-E.

Lines B-E and D-F are found similarly, by keeping the transverse stress σ_T constant at the level at B and D while increasing or decreasing σ_L, respectively.

This concludes the basic figure for shear based fiber failure.

To apply this criterion to predict fiber failure within a lamina, one would typically need to relate lamina strains to fiber strains using micromechanics. For certain types of matrix material, Hart-Smith introduces a simplifying assumption to bypass this. *Assuming strong, stiff fibers in a soft matrix, the fiber strains are simply assumed to be equal to the lamina strains*. The axial strains of the fiber and matrix are by necessity common, so no assumptions on longitudinal fiber vs. lamina strains are required. For the transverse properties this is not the case. For the assumption of *strong, stiff fibers in a soft matrix*, the transverse matrix stiffnesses will be less or equal to those of the fiber. If the transverse stiffnesses are the same, the fiber and matrix will share the same transverse strains, while for a softer matrix the fiber strain will be less than the matrix strain. Thus, according to Hart-Smith, neglecting micromechanics results in either a conservative situation, with the fibers less severely loaded because of the matrix straining more, or the two situations being equivalent when the matrix and fiber transverse properties are similar. It should be noted that this may not be conservative in the case of the strains used to calculate strain differentials being of the same sign. In this case the calculated strain differentials may be smaller than those actually experienced by the fibers. The price paid for the convenience of bypassing micromechanics is the added restriction that the criterion is only applicable to composites

with stiff fibers in soft matrices. Metal-matrix composites are excluded by this requirement while composites with more conventional matrices like epoxy are acceptable.

This assumption is adopted by Hart-Smith and the discussion which follows will resume the 1-2-3 notation customary for *lamina* principal axes, with 1 aligned with the fibers, 2 transverse to the fibers, and 3 through the thickness of the lamina. Based on this assumption, the lamina failure criterion is the same as Fig 2.3, with 1-2-3 replacing L-T-N in the axis labels and Poisson's ratios.

The basic criterion, Fig. 2.3, models a single failure mode, fiber failure by shear. The strength under this mode is assumed to be the same for tension and compression. If the values of compression and tension strength differ in experimental data it is assumed that different failure modes are present and cause the difference; e.g., micro-buckling in compression may reduce the compressive strength. These secondary modes will be accounted for by superposition of cutoffs on the basic figure. The shear failure mechanism is assumed to be associated with the larger of the experimental tension and compression strengths, hence the larger value is used in finding γ_{crit}.

At lamina level, we know of many materials for which the measured fiber direction tension and compression strengths are not the same. Micro-buckling of small-diameter fibers in compression is common, for example. The approach used by Hart-Smith to accomodate this difference is to superimpose a cut-off for each failure mechanism present. In this way fiber tensile or compressive weakness is accommodated when needed by superimposing a cut-off at the appropriate position. This is illustrated in Figs. 2.4 and 2.5.

In Fig. 2.4 the compressive failure strain is given by ε_{0c}. The cutoff line is drawn parallel to the ε_2 axis, as Hart-Smith assumes the compressive failure mechanism not to be dependent on transverse strain, as would be the case for micro-buckling of the fibers, for example. For the less common case of smaller tensile than compressive strength the cutoff may be drawn parallel to the transverse load line, if it is known that the mechanism involved is more likely to be a stress related limit (See Figure 2.5). In this way the effect of distinct failure modes are isolated to the area where they occur, without influencing failure prediction in other areas.

The criteria shown in Figs. 2.3, 2.4 or 2.5 can be directly applied as a ply-by-ply failure criterion. One aspect of the shape is however likely to draw protest from those accustomed

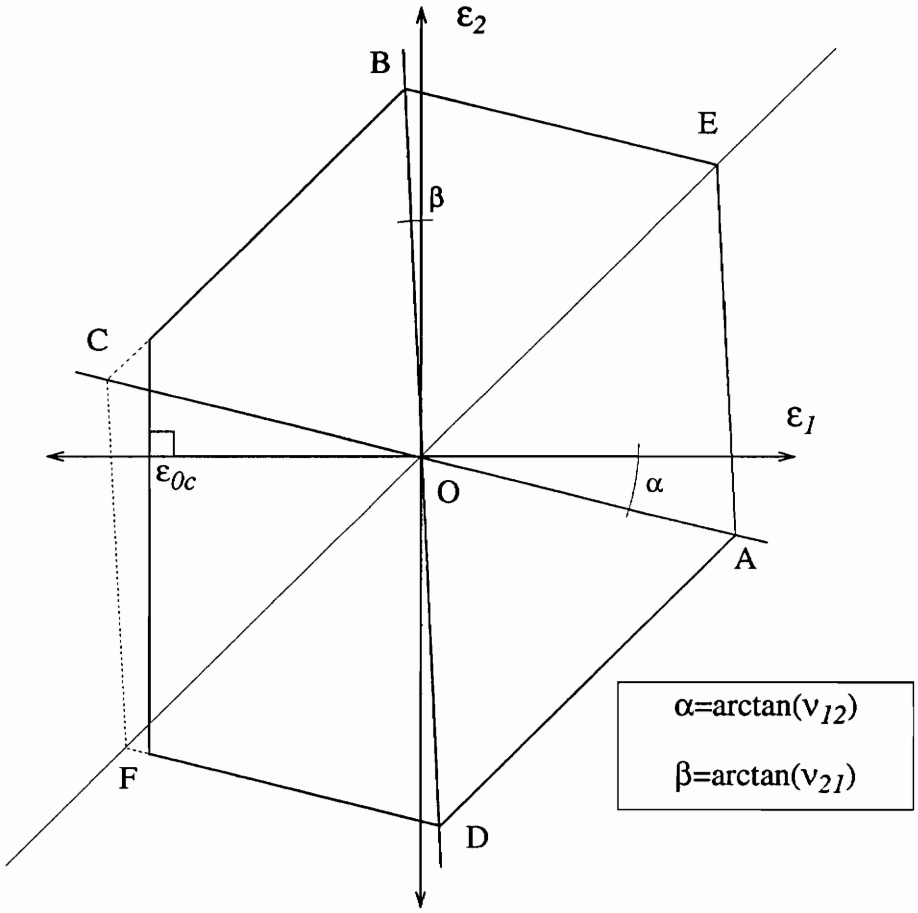

Fig. 2.4 Cutoff for low compressive strength

to the low transverse strain to failure of transversely loaded unidirectional composites. For matrix materials such as most epoxies, for example, testing coupons in the 90° direction result in failures at strains typically much lower than the strains to failure in the fiber direction. The present method would typically predict strains somewhat higher than the fiber strain in the transverse direction. Hart-Smith contends that the low strain to failure of 90° unidirectional laminates is due to the common test method which uses extremely crack-sensitive all 90° laminates. It is argued that the presence of the fibers act as severe stress raisers, particularly at the free edges, causing premature failure. A better test method is proposed in [17] where backing-out transverse properties from tests on 0°/90° laminates is proposed instead of pure 90° laminates. It is thought that the presence of the orthogonal

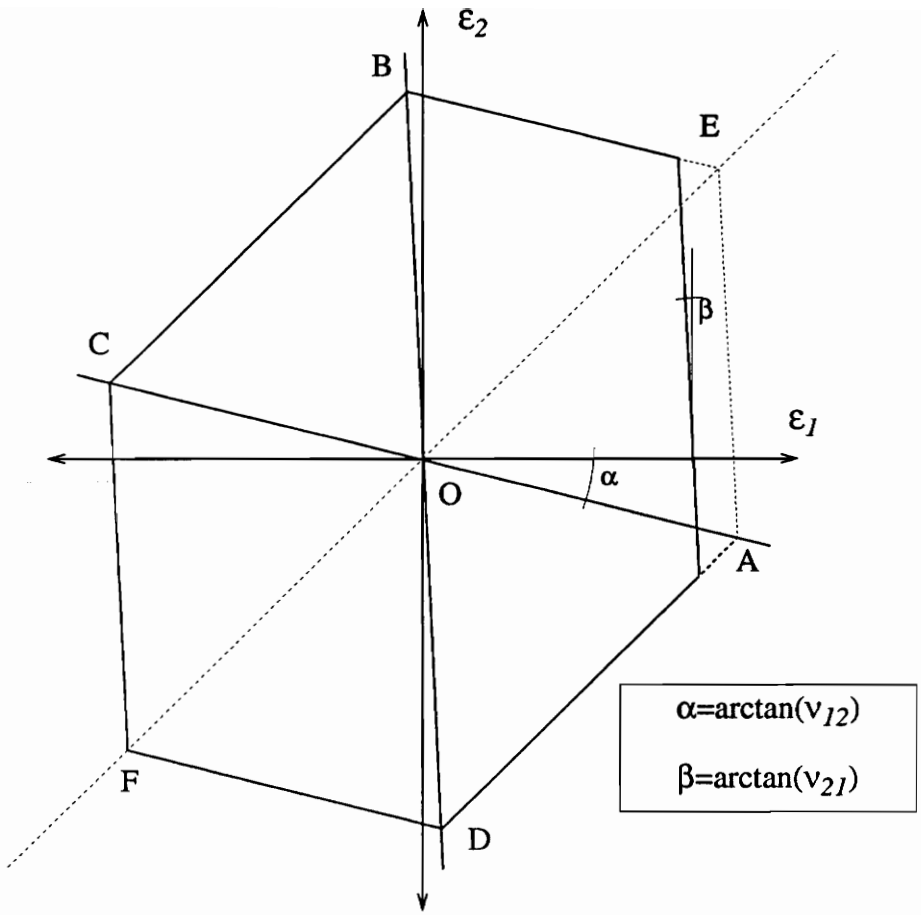

Fig. 2.5 Cutoff for low fiber tensile strength.

plies prevent premature structurally significant matrix cracking. For this reason Hart-Smith requires plies to always be used in perpendicular sets, and that the laminate be interspersed as well as possible.

Up to now only axial stresses in the fiber principal axes have been considered. Obviously, conditions arise for which the principal, (no shear stress) planes do not line up with the fibers, or equivalently shear strain in the fiber axes exist. For this case the requirement that ±45° fibers accompany all 0°/90° fibers is invoked. Recall that pure shear in one reference system translates to pure biaxial tension-compression in the set of axes at 45° to it. There would therefore always be ±45° fibers present to take the brunt of the shear loads in pure tension-compression. In addition, when considering the effect of in plane shear on the 0°/

90° layers the argument of stiff fibers in a soft matrix is used. It is expected that for soft matrices most of the shear strain will be limited to the matrix, be well below the matrix shear limit, and therefore not affect the fibers unduly. Hart-Smith states categorically that this assumption would hold for glass-, carbon- and boron-fibers in epoxy resins. Once again more exotic materials like metal matrix composites are excluded from the criterion. As a result the lamina level criterion is unbounded along the in-plane shear axis, in anticipation of fiber failures occurring in the axes at ±45° to the lamina under consideration.

2.2.3 Application of Hart-Smith criterion

When the failure envelopes for 0°, 90°, and ±45° laminae are translated into the x-y laminate coordinates, and the superimposed envelope projected on to the x-y laminate coordinates, with the 0° fibers aligned with the x-axis, etc., Fig. 2.6 results. Note that matrix failures are now typically truncated by fibers in the perpendicular direction failing first. For the case of equal tension and compression strength plotted, note also the symmetry in the tension-tension and compression-compression quadrants. Considering the effect of in-plane shear, with shear plotted along the third axis, Fig. 2.7 results. The "roof" of the figure is defined by failures of the ±45° plies, while the sides are defined by failures as shown in Fig. 2.6.

Applying Hart-Smith's criterion for in-plane loading can be done in two ways. The lamina failure criteria can be superimposed to find the laminate failure criterion, defined by the inner envelope of Fig. 2.6, and illustrated in three dimensions in Fig. 2.7, as long as the strains are uniform through the thickness. The superimposed criterion, Fig. 2.7, can be applied directly to the laminate strains of a laminate containing each of the four required fiber angles.

Alternatively, the lamina criterion, Fig. 2.3, can be applied ply by ply. This approach is used here. For a base load condition analyzed, ply level strains are computed in the fiber coordinate system 1-2. The strength ratio, R, is defined as the ratio by which lamina level strains must be multiplied to reach failure; i.e., $R_n\bar{\varepsilon}_n$, with $\bar{\varepsilon}_n$ the vector of lamina strains for lamina n, associated with a base load, will cause failure in lamina n. R_n is found for each vector of lamina strains, by finding the multiplier of the ray in the 1-2 plane formed by ε_1 and ε_2, needed to intersect the failure envelope. Shear strain, γ_{12}, is not considered at

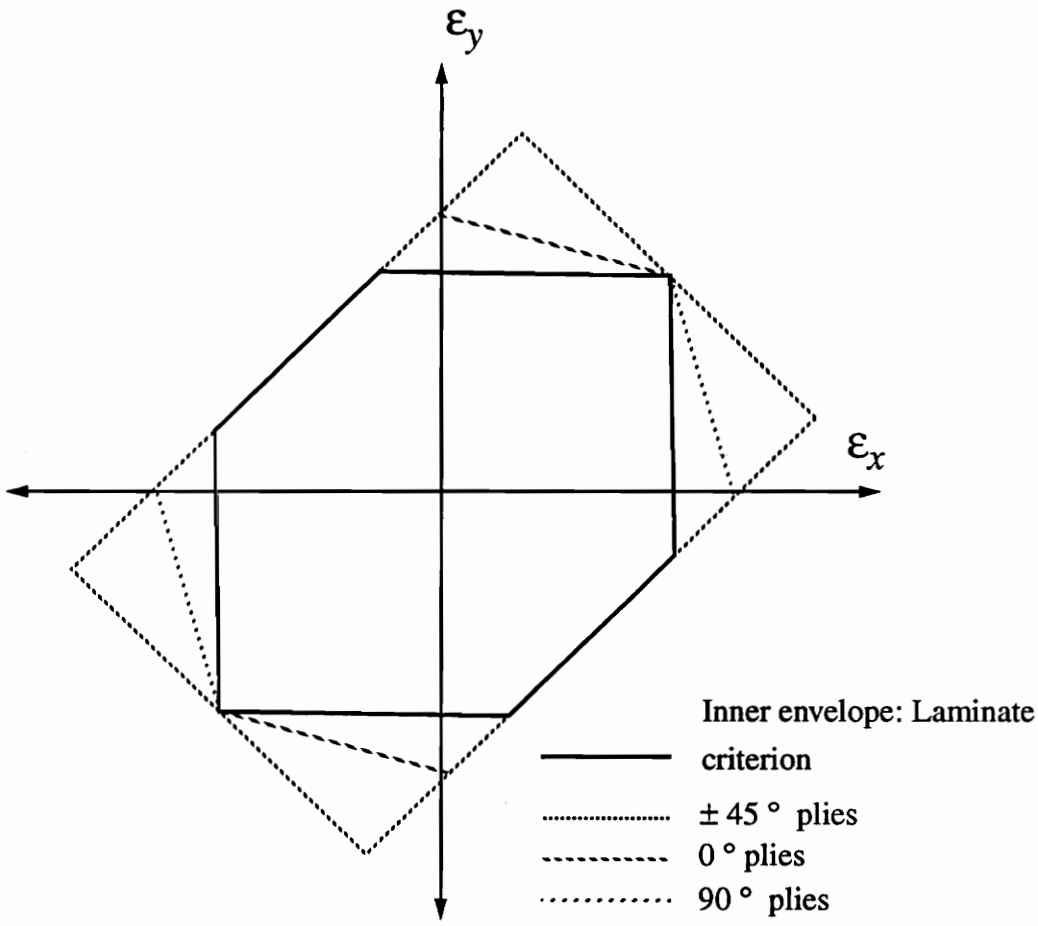

Fig. 2.6 Superposition of 0° , 90°, ±45° lamina failure criteria of Hat-Smith in laminate coordinates

the lamina level, as there must be fibers at ± 45° that carry the in plane shear in tension-compression, as explained before. Thus, $R < 1$ means the applied strain exceeds the maximum and is not allowable, $R = 1$ is failure, and $R > 1$ implies the applied strain can be increased by the factor R before failure. The strength ratio R is now calculated for each ply under the applied loading; i.e., R_n, n=1, 2 , .., *nply*, with *nply* the number of plies present. The failure ratio for the laminate is the minimum value of R_n;

$$R_{Laminate} = Min\{R_n : n = 1, ..., nply\} \qquad 2.7$$

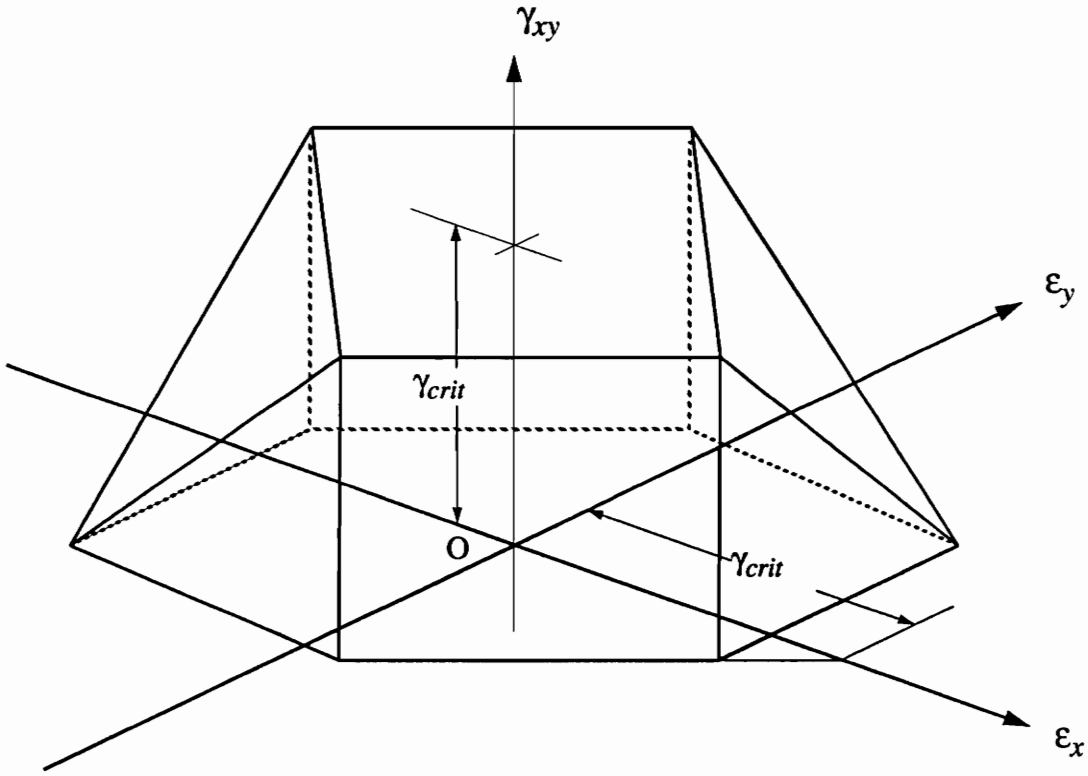

Fig. 2.7 Hart-Smith laminate failure criterion for 0°, 90° and ± 45° plies, with laminate in-plane shear plotted on the vertical axis.

i.e., the R_n associated with the ply that will fail first. The applied base load can be multiplied by $R_{Laminate}$ to find the laminate failure load level.

2.2.4 Criticism of other failure criteria by Hart-Smith

In his various papers, Hart-Smith spends considerable time explaining why he thinks other failure criteria are incorrect. In particular the notion, common to most failure theories, that it is reasonable to treat the material at lamina level as a homogeneous orthotropic body for the purpose of failure prediction, is rejected. In [17], a list of problems with the other theories is given, some of which are summarized below:

1) "The absence of residual curing stresses within a lamina"

Although it is common to calculate residual curing stresses at lamina level due to laminae contracting differently within a laminate, homogenizing the lamina leaves no opportunity to include the residual thermal stresses *within* the lamina. Hart-Smith states that for typical AS-4/3501-6 internal curing stresses in the matrix can be as high as 15-ksi tensile along the fiber and 6-ksi around the fibers. Compared to the 4-5 ksi typically needed to crack the laminate transversely, these are high stresses. Yet in the progressive failure model by Tsai, these stresses are ignored in calculating first-ply failure, which is often by matrix cracks. This method is rejected as unscientific.

2) "The drawing of smooth continuous failure curves through test data characterizing different modes of failure"

Reference is made to Hill's classical work on predicting yield for anisotropic metals, where the failure curves are smooth. Since Hill was working with a single mode of failure, this is acceptable, but the extension to non-homogeneous materials, failing under multiple failure modes, is rejected. The main reason for rejecting this idea is the fact that in these curve-fit type criteria a change in one reference strength results in change of all points on the boundary, with the exception of the other reference strengths. An example of an increased biaxial compression strength resulting from a decrease of the transverse tension strength is given.

3) "The ability of fibers to exceed their measured strain to failure."

Two points are made here. The first is that for 0° / 90° / ±45° laminates all the fibers are fully strained at the biaxial tension and compression points, as can be seen in Fig. 2.7. This implies that any additional loading would result in failure. For this reason the envelope should be pointed at the biaxial points but the Tsai-Wu first ply failure curves are blunt, implying that the ±45° fibers that are already critically strained by the 0° and 90° loads can somehow withstand additional loads. In the case of biaxial compression it is clear by looking at Fig. 2.7 that the measured fiber strains to failure will have to be exceeded for Tsai's analysis to be correct.

4) "Inability of fibers to achieve their measured strains to failure."

Looking along the biaxial line of Fig. 2.7, the envelope appears rectangular for every cross section. In addition, only on the "roof" of the figure are the 45° degree plies critically loaded. Looking at Tsai's figure along the same axis, the walls slope inward for all states of in-plane biaxial shear. This implies that for in-plane shear loads the laminate fails before the fibers reach their measured strains to failure.

5) "Failure to limit stacking sequence variations."

Hart-Smith states the well known fact that it is important to limit the number of adjacent plies with the same orientation to avoid excessive matrix cracking. Although he admits that his criterion cannot of itself predict when matrix cracking will be a problem, he places severe restrictions on the suitable laminates to avoid just that problem. The other criteria are similarly incapable of predicting severe matrix cracking, but their authors make no attempt to restrict the use of the criteria to laminates in which this will not be a problem.

This concludes the discussion of Hart-Smith's failure criterion. The criterion of Tsai will now be described.

2.3 Tsai failure criterion

The criterion described here is the latest version of the well known Tsai-Wu failure criterion for laminated composite materials. The original criterion published by S.W. Tsai and E.M. Wu in 1971 [13] is used as the starting point, with later versions found in the books of Tsai [14, ch. 11], [5, ch. 9], including expansion to include degradation and progressive failures. The version described here is found in the book "Theory of Composites Design", 1992, by S.W. Tsai [5]. This version has evolved through several steps, with Tsai's previous book "Composites Design", 1988 [14], containing a simpler version of the degradation model. Tsai proposes a multistep method of determining failure. The first step is to find the first ply to fail, based on the method of the 1971 paper [13]. After this first ply failure has been detected, an iterative procedure is used to detect the sequence and load levels of subsequent failures, with the properties of failed plies being sequentially degraded and stress distribution recalculated after each failure. This process is continued until all plies have failed, or some final failure test is satisfied. The method makes it possible, at least in

principle, not only to predict laminate failure, but also the stress-strain history of a laminate being loaded to failure, showing a decrease in stiffness as successive plies fail.

Tsai places no restrictions on the ply orientations considered, nor is the stacking sequence and interspersion of plies taken into account when applying his criterion. Analysis is simply done ply by ply. Five laminate strengths and an interaction term are needed to do the original Tsai-Wu analysis, while micromechanical data is needed for the degradation model.

The method is described in detail below, starting with the original Tsai-Wu criterion as basis followed by details of the degradation procedure and supporting arguments.

2.3.1 Basic Tsai-Wu criterion

The basic criterion is not based on a specific physical or theoretical theory of failure but is an attempt to fit experimental failure data better than previous models. Tsai writes:

> *It should be emphasized that failure criteria are empirical schemes made to fit available experimental data. Since they are not derived from fundamental principles, it is not a question of having a correct or incorrect criterion. The quadratic criterion is better because it is easier to use and more flexible.[5, p. 8-17]*

The basic criterion provides an equation with parameters dependent on both the strength properties and on interaction between some of them. Different tensile and compression strengths can be accommodated with ease. The basic equation in the stresses is given by:

$$F_{ij}\sigma_i\sigma_j + F_i\sigma_i = 1, \text{ with i, j} = 1, \ldots, 6$$

This scalar equation in the stresses describes a failure surface in three dimensional stress space, with contracted notation being used, i.e., σ_1, σ_2, σ_3 are stresses parallel to the fibers, transverse, and though the thickness of a lamina, respectively, while σ_4, σ_5, σ_6 are shear stresses. The F_{ij} and F_i terms are fourth and second order strength tensors, respectively. For the case of plane stress for an orthotropic lamina, ($\sigma_3 = \sigma_4 = \sigma_5 = 0$), the equation reduces to:

$$F_{11}\sigma_1^2 + F_{22}\sigma_2^2 + F_{66}\sigma_6^2 + 2F_{12}\sigma_1\sigma_2 + F_1\sigma_1 + F_2\sigma_2 = 1 \qquad 2.8$$

The F_{ij} terms can be found by sequentially setting different combinations of the stresses to zero and solving, using strength data for the non zero stresses. In this way we find:

For $\sigma_1 \neq 0$:

$$F_{11} = \frac{1}{XX'}$$

$$F_1 = \frac{1}{X} - \frac{1}{X'}$$

For $\sigma_2 \neq 0$:

$$F_{22} = \frac{1}{YY'}$$

$$F_1 = \frac{1}{Y} - \frac{1}{Y'}$$

For $\sigma_6 \neq 0$:

$$F_{66} = \frac{1}{S^2}$$

X and X' are the lamina tensile and compression strengths in the fiber direction, respectively, Y and Y' are the tensile and compression strengths transverse to the lamina, and S is the in-plane shear strength. The sixth term, F_{12}, cannot be determined from a uniaxial test, as it represents the interaction between failure in the 1 and 2 directions. In principle at least, it can be determined from biaxial test data, with both σ_1 and σ_2 non-zero at failure. In practice tests like these are very hard to perform and the term is usually first written in the form:

$$F_{12} = F_{12}^{*} \sqrt{F_{11}F_{22}}$$

and F_{12}^{*} then chosen empirically. Tsai recommends that the value $F_{12}^{*} = -0.5$ be used, based on arguments on the admissible range for the term [5, p. 8-11].

Due to the large anisotropy in strength for composites a plot of this criterion in stress space has a very elongated shape. It is therefore more commonly plotted in strain space and a typical shape is shown in Fig. 2.8. The points labeled A and C are the fiber direction

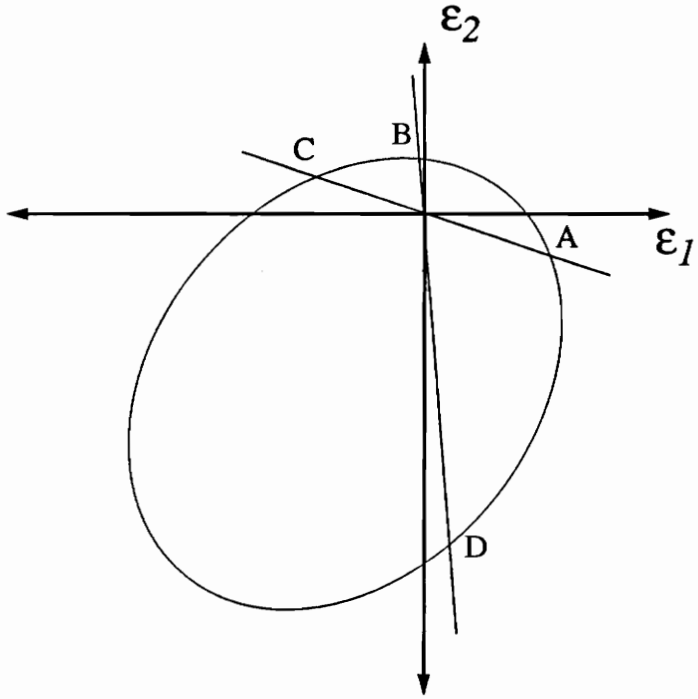

Fig. 2.8 Tsai-Wu first ply failure criterion in strain space.

tension and compressive failure points, respectively, and B and D are the transverse tension and compression failure points. Thus, the failure envelope passes through the points defined by uniaxial lamina failure in both the fiber and transverse directions. The envelope also passes through the shear failure points, and has a similar shape to that in Fig. 2.8 when plotted for the shear axis replacing one of the axes in Fig. 2.8.

In order to find the combination of stresses that will cause failure the strength ratio R, is introduced, as discussed in section 2.3. Each of the applied stress components is multiplied by R and the value that causes failure is found. Substitute $\sigma_i^{max} = R\sigma_i^{applied}$ into Eq. 2.8 to find:

$$[F_{ij}\sigma_i\sigma_j]\,R^2 + [F_i\sigma_i]\,R - 1 = 0 \qquad 2.9$$

which is a quadratic equation in R, σ_i's being the applied stresses. Solving for the positive quadratic root of R provides the ratio by which each of the applied stress values must be multiplied for failure level to be reached. Equivalently, if we apply a constant ratio of base loadings, $N_x : N_y : N_{xy}$, for example, multiplying each by R will generate failure. To find the first ply failure load for a *laminate*, a base load vector is applied, the stresses in each ply calculated, and the positive root of R in Eq. 2.9 is computed in each ply. First ply failure load is found by multiplying the base load vector by the *minimum* value of R in the laminate.

2.3.2 Tsai progressive failure model.

The need to extend Tsai-Wu to include degradation and progressive failures stems from the fact that the low transverse tensile strain to failure of unidirectional laminae, measured in experiments, is typically not observed for laminates. For a 0°/90° specimen in pure tension, the Tsai-Wu criterion would predict failure at close to the transverse strain to failure for a lamina, as was input in the transverse strength Y. This would for many matrix systems, for example the epoxies, result in failure being predicted well before the fiber and therefore final failure is reached, and with the specimen still structurally intact. In order to reconcile this measured lamina failure strain in the transverse direction with the absence of drastic failure for laminates, a progressive degradation scheme has been developed. The simplest version of this would be to set the matrix properties to zero in the first ply failure ply, redo the analysis, find next ply failure, set properties to zero, and so on. This strategy does however not match with reality, as the matrix retains much of its load carrying capability beyond the predicted first ply failure point. Instead, Tsai has developed a scheme to degrade the matrix-dominated properties to typically 20% of their intact values, once first ply failure has been reached.

The flowchart in Fig. 2.9 gives an outline of how the progressive degradation scheme is implemented. To start first ply failure is calculated as described before. If the transverse normal strain in the critical ply is positive, i.e. $\varepsilon_2 > 0$, it is *assumed* that matrix cracks have formed. Failure is *defined* as a matrix failure, and the matrix properties degraded in the critical ply. If $\varepsilon_2 \leq 0$, it is assumed that the matrix has not cracked, and fiber failure is *assumed*. Fiber properties are then degraded in the critical ply. After the degradation step, the stresses or strains in the plies are recalculated for the laminate with mixed baseline and degraded properties, and Tsai-Wu applied again. Once again the transverse strain is

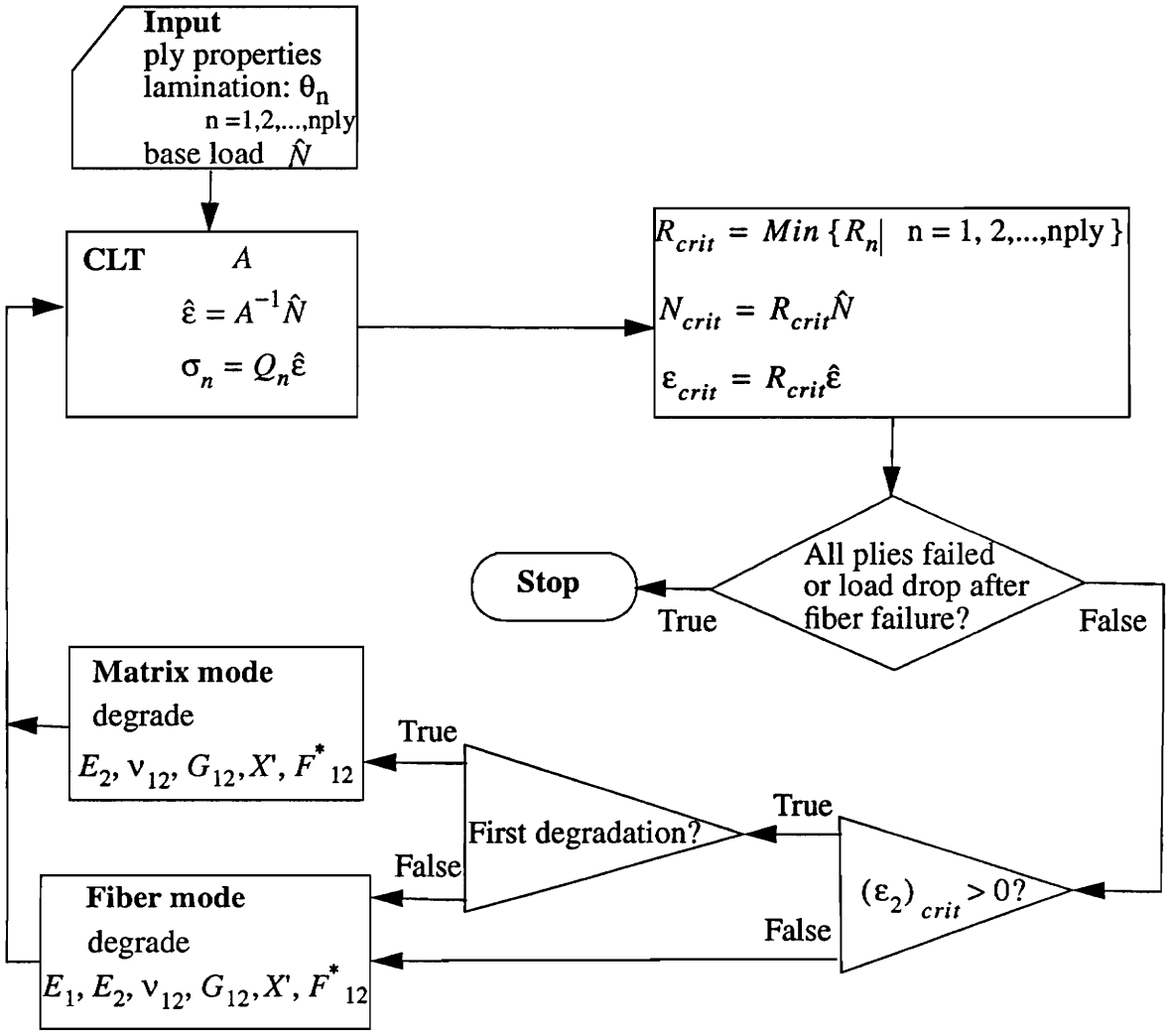

Fig. 2.9 Selective and progressive ply-by-ply degradation algorithm for in-plane, proportional loading of symmetric laminates (no bending). Adapted from Tsai [5].

checked and degradation performed. If a critical ply has had its matrix properties degraded before, and has a positive transverse strain, a fiber failure is now defined. This sequence of degradation and reanalysis is performed until some stopping criterion for final laminate failure is satisfied. One may simply let the analysis continue until all plies have reached fiber failure. Alternatively, the first ply to reach fiber failure, or the first time a subsequent failure load is less than the present value may be taken as final laminate failure. In the present study, laminate failure is defined as the fiber failure leading to a drop in the load.

Two different types of degradation are used, a matrix mode and a fiber mode. The degradation model is presented next.

2.3.3 Tsai degradation model

The matrix mode of degradation is based on the formation of microcracks in the matrix of a lamina loaded in transverse tension. The loss of stiffness in the lamina is modeled by degrading the matrix dominated properties, using micromechanics equations.

Modified rule of mixtures equations are used to find transverse properties, as given below:

$$\frac{1}{E_2} = \frac{1}{(1+\upsilon_2^*)}\left[\frac{1}{E_{f2}} + \frac{\upsilon_2^*}{E_m}\right] \qquad 2.10$$

$$\frac{1}{G_{12}} = \frac{1}{(1+\upsilon_{12}^*)}\left[\frac{1}{G_{f12}} + \frac{\upsilon_{12}^*}{G_m}\right] \qquad 2.11$$

with E_2 and G_{12} the lamina transverse and in-plane shear moduli, respectively. The quantities with subscripts f and m refer to fiber and matrix properties, respectively, with E_{f2} the transverse fiber stiffness, etc. The property υ_i^* is related to stress partitioning parameters, η_i, defined in [18, p. 393], which account for the different fiber and matrix stresses at micromechanical level for a transversely loaded fiber-matrix system. The η_i's are defined from

$$\sigma_{m2} = \eta_2 \sigma_{f2}$$

and

$$\tau_m = \eta_{12} \tau_{f12}.$$

The value of the η_i terms are mainly dependent on the geometry of the fiber-matrix system, and can be treated as empirical constants for most unidirectional fiber-matrix systems. Tsai suggests the values $\eta_2 = 0.5161$ and $\eta_{12} = 0.3162$.

The υ_i^*'s are defined as:

$$\upsilon_2^* = \eta_2 \frac{v_m}{v_f}$$

$\upsilon_{12}^* = \eta_{12} \frac{v_m}{v_f}$, with v_m and v_f the matrix and fiber volume fractions, respectively.

The quantities E_{f2} and G_{f12} are typically not available but are back-calculated from Eq. 2.10 and 2.11, using undegraded properties. The basis of the degradation scheme is that only the matrix modulus E_m is degraded, and the influence on the other properties calculated from the equations given. The *matrix degradation factor*, E_m^* is defined as

$E_m^* = \frac{E_m^{degraded}}{E_m^{baseline}}$, and is treated as an empirical constant, and the value suggested by Tsai is listed in Table 2.1. To calculate $E_2^{degraded}$ and $G_{12}^{degraded}$, E_m^* is used to degrade E_m and G_m in equations 2.10 and 2.11 to find:

$$\frac{1}{E_2^{degraded}} = \frac{1}{(1+\upsilon_2^*)}\left[\frac{1}{E_{f2}} + \frac{\upsilon_2^*}{E_m^* E_m}\right] \qquad 2.12$$

$$\frac{1}{G_{12}^{degraded}} = \frac{1}{(1+\upsilon_{12}^*)}\left[\frac{1}{G_{f12}} + \frac{\upsilon_{12}^*}{E_m^* G_m}\right] \qquad 2.13$$

where G_m is also degraded by direct multiplication by E_m^*. The degradation factors E_2^* and G_{12}^* are defined in the same way as E_m^*. In addition to degradation of matrix-dominated stiffness properties, the fiber direction compressive strength X', is degraded. This is based on the argument that the compressive strength will be affected by loss of stiffness of the matrix as the fibers will be more likely to buckle. This is quantified by a power law equation:

$$\frac{X'^{degraded}}{X'} = \left(\frac{G_{12}^d}{G_{12}}\right)^n = (G_{12}^*)^n \qquad 2.14$$

The exponent n is an empirical constant. Finally the term F_{12}^* and the Poisson's ratio ν_{12} are degraded by multiplying with E_m^*.

Fiber degradation models fiber failures in a ply. A similar approach to matrix degradation is used. In this case both the fiber and matrix properties are degraded by application of an empirical fiber degradation factor E_f^*. E_1 is degraded by direct multiplication with E_f^*. E_2 and G_{12} are degraded by multiplying the matrix properties, E_m and G_m in equations 2.12 and 2.13 by E_f^* instead of E_m^*. In addition the term F_{12}^* and the Poisson's ratio ν_{12} are degraded by multiplying with E_f^*. X' is degraded as in Eq. 2.14, with the G_{12}^* value calculated from E_f^* now used.

As mentioned, the stress partitioning parameters, η_2 and η_{12}, the degradation factors E_m^*, E_f^*, and the exponent n are empirical constants. The values for these are given by Tsai for a number of materials. For T300/5208 these are reported in Table 2.1.

TABLE 2.1 Empirical constants associated with Tsai degradation model.

Empirical constant	Value
η_2	0.5161
η_{12}	0.3162
E_m^*	0.15
E_f^*	0.01
n	0.1

An overview of the matrix degradation scheme and typical values of degradation is given in Table 2.2, and the same information for fiber degradation is given in Table 2.3. Additional properties mentioned are the properties needed to apply the degradation model, beyond those needed to do first-ply failure prediction.

TABLE 2.2 Summary of Tsai matrix degradation model.

Property	Degradation method	Additional properties needed	Typical degradation factor
E_1	None	None	1.0
E_2	Micromechanics, Eq. 2.12	E_m, v_f, v_m, η_2	0.243
ν_{12}	Direct multiplication by E_m^*	None	0.15
G_{12}	Micromechanics, Eq. 2.13	E_m, v_f, v_m, η_{12}	0.206
X	None	None	1.0
X'	Empirical, Eq 2.14	As for G_{12}, n	0.85
Y	None	None	1.0
Y'	None	None	1.0
S	None	None	1.0
F_{12}^*	Direct multiplication by E_m^*	None	0.15

TABLE 2.3 Summary of Tsai fiber degradation model.

Property	Degradation method	Additional properties needed	Typical degradation factor
E_1	Direct multiplication by E_f^*	None	0.01
E_2	Micromechanics, E_f^* used in Eq.2.12	E_m, v_f, v_m, η_2	0.018
ν_{12}	Direct multiplication by E_f^*	None	0.01
G_{12}	Micromechanics, E_f^* used in Eq. 2.13	E_m, v_f, v_m, η_{12}	0.015
X	None	None	1.0
X'	Empirical, Eq. 2.14	As for G_{12}, n	0.66
Y	None	None	1.0
Y'	None	None	1.0
S	None	None	1.0
F_{12}^*	Direct multiplication by E_f^*	None	0.01

This concludes the discussion on failure criteria. The next chapter details the analyses and optimization used in designing optimal experimental laminates.

Chapter 3 : Analysis and Optimal Test Design

3.1 Introduction

The objective of this study is to find conditions that optimally differentiate between the predicted failure loads of two composite failure criteria. The theoretical methodology for finding such conditions will be addressed here. As is typical in optimization problems the parameters to be optimized are referred to as *design variables* and these may include applied stresses, load combinations or ratios, laminate ply angles, or combinations of these. The *Objective function* is the ratio of failure loads for the two criteria. *Constraints* on the problem may take many forms, for example limitations on ply angles allowed, lim-

itation of load types allowed, limiting a laminate's susceptibility to delamination, etc. In this way the most general problem may be stated:

Find the extremum of $F(\Omega, N) = \dfrac{R_{Hart\text{-}Smith}}{R_{Tsai}}$,

subject to $\Omega \in C$,

with Ω the vector of design variables defining the laminate, and N the vector of design variables defining the applied loading. C is the constrained set containing the feasible laminate designs. The R's are the strength ratios defined in Chapter 2, for the two failure criteria; i.e., for the laminate in question, $NR_{Hart\text{-}Smith}$ and NR_{Tsai} cause failure, respectively.

The objective of finding conditions that optimize the ratio of predicted failure loads may be pursued for two reasons. The first is to gain *theoretical* insight into the differences between the two failure criteria. This may be done by selecting the most general set of loads and laminate design variables possible under the constraints of the theories. This theoretical optimum will be important as it provides insight into the area of greatest disagreement, and may suggest the strengths and weaknesses of the two theories. In this comparison the extremum values of the failure ratios are of interest. However, since different parts of the criteria represent different types of loading, it is also important to investigate local optima in the design space. This may be achieved by limiting the load parameters used, for example only in-plane loads with no shear may be selected, or only longitudinal loads of a certain sign.

The second reason for performing the optimization is to find a set of conditions under which it is possible to conduct an experiment. Once the first problem is solved, that of finding general optimum loads and lamination angles, there is no guarantee that it will be practical to achieve the required conditions in an experiment. Deciding on the parameters suitable for doing a test may be based on the complexity of test that can be conducted and on the aspect of the criteria under investigation. Use of data obtained in the more general comparisons may guide the search for interesting tests. The approach used here, therefore, is to first find a theoretical limit or limits for F and then, based on information gained decide on a practical test type, define a new optimization problem, and solve to find the optimum experiment.

The optimization problem is solved in two steps. The first step is to relate design variables to the objective function and the second is to modify the design variables so as to optimize the objective function. The steps are referred to as the analysis and optimization problems, respectively, and are described next.

3.2 Analysis

As the object of this study is the experimental comparison of failure criteria it may be argued that the state of strain in the laminates tested should best be spatially homogeneous, so that failure is more likely to be a global, as opposed to a local, event. The criterion of Tsai, for example, recalculates the strain distribution each time a ply has "failed", even if the failure is no more than matrix cracking. If the specimens therefore had large gradients in the global or ply level strains, the failure process may be too complicated to predict accurately. In the case of Hart-Smith, even though he states that his criterion is suitable for use on a ply-by-ply basis, he certainly advocates it most strongly for laminates where the strains for the different plies are the same. In the extreme case where there are strong strain gradients through the thickness, his argument of plies in the perpendicular direction stabilizing matrix cracking in transversely loaded plies may be invalid.

An example of a state of strain somewhat unsuitable for experimental verification may be found in the paper by Haftka and Kao[4]. A rectangular laminated plate with a hole is analyzed with the finite element method, and conditions for a theoretical large failure load ratio are found. In their study this was used as an example for doing the analysis, not as a suggested test specimen. It will be instructive, however to consider a test on such a specimen. The geometry implies that the theoretical critical conditions for failure are reached locally, in a specific element. For the actual plate loaded to the same level the failure would be a *very* local event, and may not necessarily be detectable. Predicting progressive failure using the finite element scheme to calculate local degradation and corresponding redistributed loads would require an extremely fine mesh. Therefore, from the point of view of obtaining reliable tests, a more or less homogeneous state of strain throughout the laminate is advantageous.

For the reasons given, laminate-load combinations will be limited to those yielding spatially homogeneous strain fields. For such strain fields a simple theory, such as classical

lamination theory (CLT), [8, pp. 147-156], will be suitable. More advanced methods are used only where needed to verify these results.

When only using in-plane loading and symmetric laminates the middle surface strains, $\varepsilon_x{}^0$, $\varepsilon_y{}^0$ and $\gamma_{xy}{}^0$ may be related to the applied stress resultants, N_x, N_y, N_{xy}, by the well known extensional stiffness matrix, A [8, p. 155]. That is,

$$\begin{bmatrix} N_x \\ N_y \\ N_{xy} \end{bmatrix} = \begin{bmatrix} A_{11} & A_{12} & A_{16} \\ A_{12} & A_{22} & A_{26} \\ A_{16} & A_{26} & A_{66} \end{bmatrix} \begin{bmatrix} \varepsilon_x^0 \\ \varepsilon_y^0 \\ \gamma_{xy}^0 \end{bmatrix}, \qquad 3.1$$

For in-plane loading of symmetric lamintes, ply strains and middle surface strains are the same, with lamina strains still given in the laminate coordinates. The usual rotation to lamina coordinates and application of the lamina stress-strain law yields ply stresses. A more complete treatment of this well known theory may be found in [8, ch. 4].

Once lamina strains are known in each ply, a prediction of the failure load can be made. This was explained in detail in chapter two. Recall that for both criteria a strength ratio R is calculated for each ply, and the lowest value obtained in the laminate can be multiplied directly by the applied load vector to find laminate failure loads. In the case here, since the load vector for the two failure analyses is the same, the ratio of the two minimum R values is the ratio of the failure loads, F.

3.3 Optimization

The optimization problem has been stated in the introduction to this chapter. Before deciding on an optimization technique it is necessary to determine the nature of the problem. The design variables are a combination of laminate and load variables. The ply angle variables will be discrete, as the possibilities are limited to four basic angles at 45° to each other. The load parameters are continuous variables, but may be approximated by discrete numbers if a sufficiently fine discretization scheme is used. The objective function is a nonlinear function of the design variables, and is in addition non-smooth. We may assume this based on the fact that Hart-Smith's criterion is a non-smooth figure in strain space, and because the ply where failure is initiated can change during the optimization. Con-

straints on the problem include limitations on ply-angles present and possibly limitations due to delamination parameters.

The problem is fairly complex, with discrete design variables, a nonlinear, non-smooth objective function and complex constraints. In addition there is no reason to expect that local optima will not exist. Conventional optimization techniques employing searches based on gradients cannot be expected to be of much use here.

An optimization process suitable for problems of this nature is however available. Genetic algorithms are suitable for optimization problems with discrete design variables and nons-mooth or disjoint design spaces. These algorithms will be used in the general optimization problem and are described below.

3.3.1 Genetic Algorithms

Genetic algorithms [20], [21], and [22], are search techniques mimicking the biological processes of evolution. The algorithms apply Darwin's principle of "survival of the fittest" to populations of designs, creating new generations by selectively using good characteristics from old designs. The method is inherently probabilistic. Some of the main features of the algorithms are:

- Discrete design variables are commonly used.
- No derivative information is used
- A population of optimal or near optimal designs is produced.
- The method is insensitive to discontinuous or disjoint design spaces
- The method is insensitive to the meaning of design variables.

The algorithms work with a set of designs and performs genetic operators on the designs to iteratively improve the set. The process is applied until a set containing a suitably good design is obtained. The process is described in more detail below.

The basic form in which the algorithm represents and works with design variables is a string, also called a *person*, which contains representations of individual design variables strung together. Each person represents a design. This is analogous to chromosomes used in biology to store genetic information. Inside each person a single design variable can be

coded by either a single number, or bit, or by a sub-string of numbers. For example a binary string may be used to represent a design with three design variables:

$$1011|\,01101|\,11$$

Representing x_1=1011, x_2=01101, x_3=11. Note that the sub-strings need not be of the same length. Each design variable takes a certain position in the string and is represented by a binary string. Instead of binary numbers another base may be used. To represent the four ply angles, 0°, 90° 45° and -45° base 4 numbers are appropriate, with each number representing a ply angle:

$0 \rightarrow 0°$,

$1 \rightarrow 90°$,

$2 \rightarrow 45°$,

$3 \rightarrow -45°$,

for example. If a continuous variable must be coded, it must be discretized first. For example to code a base n variable with range from x_i^L to x_i^U with a required minimum increment of x_{incr}, m numbers are needed in the sub string, with m obtained from [21]:

$$n^m \geq \left[\frac{(x_i^U - x_i^L)}{x^{incr}} + 1 \right], \qquad 3.2$$

For example to code a base 4 variable with range -5 to 5 with a required increment of 0.2, 3 digits are needed, giving an actual increment of 0.1587.

The genetic operators applied to a population are known as *selection*, *crossover* and *mutation*. To start the process, a random set of designs is produced, also called a *population*, with each person in the population representing a design coded as a random selection of design variables. The initial population of designs is then analyzed, and for each design an objective function value is found. The designs are each assigned a *relative fitness* number, corresponding to a measure of the designs objective function, or relative worth. The fitnesses are generally numbers adding up to one, and may simply be the normalized objec-

tive functions. Other means of ranking are often used, for example the designs may be ranked from best to worst, and the normalized position in the rank used as fitness.

Once relative fitnesses have been determined, *selection* is performed. A new population is randomly selected from the old one, but the selection is biased towards designs with high fitness. This may be visualized best by imagining repeatedly spinning a roulette wheel to randomly select a new population from the old, with sectors of varying area corresponding to the fitness of each original design. A new population of designs, biased towards the good ones in the old set, is found in this way.

In order to improve the genetic material available, *crossover* is now performed on the new set. Members of the population are paired of randomly to participate in crossover, and this operator is applied with a high probability. The pairs are called parents and the offspring, not surprisingly, children. This operator is analogous to biological organisms reproducing to form new organisms that share some of the properties of the parents. First a crossover point, or points are randomly selected, and the bits of each string interchanged after, or before the crossover point. An illustration of crossover is shown below.

Crossover point ↓

Parent 1 0123| 333

Parent 2 2222| 123

After crossover:

Child 1 0123| 123

Child 2 2222| 333

More than one crossover point is also possible. The idea behind crossover is to provide new combinations of genetic material, from a population already selected for its good characteristics, in the hope that some of the good parts will combine to yield even better designs. Of course the bad parts may also combine, but these will be filtered out in the next selection step.

As can be seen, the steps so far work exclusively with the bits making up the original population. There is no guarantee that, even by recombining them in all possible combina-

tions, that the entire design space can be represented. In addition the selection process may find individuals that dominate the current population after a number of cycles. For this reason, and again mimicking nature, the operator of *mutation* is introduced. This operator is applied with a very low probability to randomly select a bit, and randomly change its value. This is illustrated below:

Random mutation site :	↓
Randomly selected person :	1023012
Person after mutation :	1023312

These three operators are applied sequentially until a stopping criterion is satisfied. For example it may be required that the best design in each successive population not change for a certain number of cycles. Alternatively, one may simply limit the number of cycles allowed.

As in any optimization process constraints may have to be imposed. In genetic algorithms this is most commonly achieved by designing the coding such that only feasible designs are possible, or if this is impossible, by a penalty function approach. A infeasible design may have its objective function penalized by multiplying by a penalty parameter, so as to discourage selection in the next round.

Due to the probabilistic nature of the search it is quite possible that a good design may be encountered, but not selected in the next round, and lost. To counter this possibility, an *elitist* strategy may be followed, which monitors each cycle, and keeps track of the best design to date in a separate register. As applied here this separate register was offered for selection based on a frequency determined by the operator of the code. It was found that using a "pure" elitist strategy, with the elite being offered every cycle often leads to premature domination of the population by one design. For this reason the elite design was only offered for selection every few cycles, so as to allow the search to move away from the previous best, but "remind" it periodically of previous good designs, in case the new search area proves unproductive.

It can be seen that the only requirements for an optimization problem to be analyzed by a genetic algorithm are that the design being optimized can be coded as a string of discrete design variables. For a particular design an objective function evaluation must be possible, and a test for feasibility of a design must exist when needed. The nature of the problem, be it nonlinear, disjoint, or nonsmooth is not important.

Solution of the problem at hand is now described. In the following section nominal material properties found in [5] for T300-5208, close to the intended test material, are used. In addition, hygro-thermal effects are ignored.

3.3.2 Optimization of the general problem

As stated in the introduction the theoretical optimum may be found by using the most general set of design variables for the problem. In-plane loads only will be considered, as out-of plane loads, with strains varying through the thickness, may violate Hart-Smith's assumption that transverse fibers support matrix failures in adjacent plies. The use of in–plane loads only reduces the complexity of the optimization for another important reason. As lamination *sequence*, as opposed to *ply content* has no effect on the in–plane response of symmetric laminates, it is sufficient to simply find the number of plies in each direction. The laminate is limited to the four basic ply angles required by Hart–Smith; 0°, 90°, 45°, and –45° and is required to be balanced and symmetric. In addition, at least 12.5% of fibers are required in each of the four directions. This naturally leads to use of laminates with multiples of 16 plies, as a 16-ply laminate will satisfy the ply-percentage constraint simply by having at least a single ply in each direction in the symmetric sub–laminate. The optimization is, therefore, limited to in-plane loads on a symmetric, balanced 16-ply laminate, with fibers in each of the four basic directions.

The most general selection of load design variables may be the selection of the three lamina in-plane stresses or strains.This approach was used by Haftka and Kao [4] in their comparison of the criteria of Tsai-Wu and Tsai-Hill. They note that in this manner a theoretical upper and lower bound on the failure ratio may be found. In the case under consideration here using *lamina* stresses are not appropriate. Both criteria predict *laminate* failure and, for example in the case of Tsai, degradation of a transversely loaded single lamina is not defined. Hart-Smith requires that plies in four main directions be present. For this case a vector of normalized in-plane stress resultants $\hat{N}$, with

$$\hat{N} = \begin{bmatrix} N_x \\ N_y \\ N_{xy} \end{bmatrix}, \text{ and } \sqrt{N_x^2 + N_y^2 + N_{xy}^2} = 1$$

is used.

For solution by genetic algorithm the design variables must be coded as discrete numbers. The laminate variables are by nature integers, but the loads need to be discretized. In this case where only the ply content and not the stacking sequence is important the number of possible laminates is limited to 9. This may suggest a base 9 system be used for the genetic algorithm coding. However, this means the laminate is represented by a single number in the optimization string. It is more customary in coding of designs to use longer strings, allowing more chances of mixing the various properties. Using a base 3 system, the nine candidates can be coded most efficiently, as two digits in base 3 can exactly accommodate the designs. However, as a code using base 4 was available from preliminary work on the problem, it was decided to continue with this coding. Using a sub-string of two base 4 numbers, 16 laminates can be represented. The scheme code the designs is shown in Table 3.1.

The "Jump" parameter in Table 3.1 was used to handle the fact that more than the required nine designs can be coded by this sub-string. The Jump parameter was used to entirely skip the objective function evaluation for designs for which Jump = 1, and to assign an uncompetitive objective function value to these unoccupied codings. This ensures the design is likely to be filtered out by selection. In this way computational cost is reduced, as infeasible designs are identified before analysis begins, and withdrawn from that step.

The three normalized stress resultants can be represented by two spherical coordinate parameters ϕ and ω, with N_x, N_y, and N_{xy} given by:

$N_x = \cos(\phi)\cos(\omega)$;

$N_y = \cos(\phi)\sin(\omega)$;

$N_{xy} = \sin(\phi)$.

TABLE 3.1 Coding of laminate design variables.

Coding	±45°ply stacks	0° plies	90° plies	Jump parameter
00	1	1	5	0
01	1	2	4	0
02	1	3	3	0
03	1	4	2	0
10	1	5	1	0
11	n/a	n/a	n/a	1
12	n/a	n/a	n/a	1
13	n/a	n/a	n/a	1
20	2	1	3	0
21	2	2	2	0
22	2	3	1	0
23	n/a	n/a	n/a	1
30	3	1	1	0
31	n/a	n/a	n/a	1
32	n/a	n/a	n/a	1
33	n/a	n/a	n/a	1

with $\phi = 0°$ to $90°$ and $\omega = 45°$ to $225°$ providing the necessary ranges for the stress resultants when exploiting symmetry. The physical meaning of the parameters is that ϕ controls the ratio of axial to shear loads, and ω controls the ratio of x– and y–direction axial loads. These parameters are discretized by using base 4 numbers with three digits used for ϕ and four for ω. This results in ϕ and ω being discretized with increments of 1.429° and 0.7059°, respectively.

The total length of the coding is nine digits, two digits for the laminate, three for the axial to shear ratio, and four for the axial load ratio. The design space therefore consists of approximately 2.6×10^5 designs.

In the solution of the problem by genetic algorithm, the population size was chosen as 12 persons, with 100 cycles typically needed to obtain convergence, meaning less than 0.5% of the design space is typically sampled. This is still on the high side for genetic algorithms, but the design space is of fairly modest proportions, and larger problems often lead to declining percentages of the design space needed to be sampled.

Optimal designs obtained by genetic algorithm are shown in tables 3.2 and 3.3.

TABLE 3.2 Laminate–load combinations minimizing failure load prediction ratio *F*. Solution by genetic algorithm.

±45° plies	90° plies	0° plies	Nx	Ny	Nxy	Iterations	Failure load ratio, *F*
1	2	4	-0.7962	-0.6051	0.0	250[a]	0.40080
2	2	2	-0.7493	-0.6622	0.0	68	0.40081
1	3	3	-0.7654	-0.6436	0.0	86	0.40082
1	1	5	-0.9288	-0.3697	0.0249	70	0.40082
1	2	4	-0.8384	-0.5445	0.0249	70	0.40087

a Execution halted at 250 iterations.

TABLE 3.3 Laminate–load combinations maximizing failure load prediction ratio *F*. Solution by genetic algorithm.

±45° plies	90° plies	0° plies	Nx	Ny	Nxy	Iterations	Failure load ratio, *F*
1	1	5	-0.4384	0.7871	0.4339	58	1.8897
1	1	5	-0.4189	0.7977	0.4339	55	1.8882
1	1	5	-0.3791	0.8173	0.4339	350[a]	1.8854
1	1	5	0.1104	0.9148	0.3884	200	1.8739
1	1	5	-0.285	0.8292	0.4783	115	1.8726
1	1	5	0.0197	0.9113	0.4113	88	1.8709

a Execution halted at 350 iterations.

Note that a number of near–optimum cases are presented, which is a feature of genetic algorithms.

The greatest ratio of predicted failure load occurs in the minimization case, representing areas of the failure criteria where the Tsai failure load is higher than the Hart-Smith failure load. The loadings are all characterized by the absence or virtual absence of in-plane shear, and by biaxial compression. This is no surprise as the two criteria differ greatly in the compression–compression quadrant. It is interesting to note that in the cases where the laminate contains equal numbers of plies in the 0° and 90° directions, the loading is close to pure biaxial compression, but not exactly so. This was apparent anomaly was investi-

gated by calculating the value of F for pure biaxial compression for the second laminate in Table 3.2. The result confirms the optimization, for a $[\,0_2\,/\,90_2\,/\,\pm45_2\,]_s$ laminate the value of F under pure biaxial compression, (N_x/N_y=1), is 0.41002,as compared to 0.40081 for N_x/N_y=1.1315, as in Table 3.2.

A second check on the optimization result was performed by calculating the failure load ratio F, for the first laminate in Table 3.2, when varying the parameter ω and keeping ϕ fixed at zero. Using an increment in ω of 0.01° the lowest value of F was found to be 0.40080381, at $N_x : N_y : N_{xy}$ equal to -0.79632 : -0.60488 : 0.0. This result is very close to the one found in the genetic algorithm search, and is within the resolution of the discretization scheme used.

The reason for the large difference in compression-compression predictions for the two criteria is illustrated in Fig 3.1. The lamina failure envelopes of Hart-Smith and Tsai are drawn to scale, and both the Tsai first-ply envelope and the envelope found when using matrix degradation are included. It is obvious that the largest difference in predicted failure occurs in the compression-compression quadrant. Hart-Smith's envelope is symmetric in compression-compression and tensile-tensile strains to failure, when the fiber direction tensile and compressive strains to failure are the same. In the case of Tsai's criterion, however, even though the fiber direction tensile and compressive strains to failure are the same, the envelope is not symmetric in compression-compression and tension-tension. Different *transverse* tensile and compressive strains to failure cause the figure to become unsymmetric. This can be seen in Fig 3.1, where the fiber direction strains to failure are equal, but the transverse strains to failure are not. The apparent anomaly that reducing the transverse tension strain to failure results in a predicted increase in compression-compression strain to failure is one reason why Hart-Smith rejects Tsai's criterion as unscientific [17].

In Table 3.3 the results of maximization are presented. Designs here represent cases where Hart-Smith failure load is higher than Tsai failure load. All loadings are characterized by unequal axial loads, combined with a significant in-plane shear load. The characteristic of the failure criteria exploited here is the treatment of in-plane shear. Hart-Smith maintains that adding in–plane shear to laminates already critically loaded by axial loads does not reduce the axial load carrying capability, see Fig. 2.7 in Chapter 2. Tsai's criterion always reduces the axial capacity for increased in-plane shear.

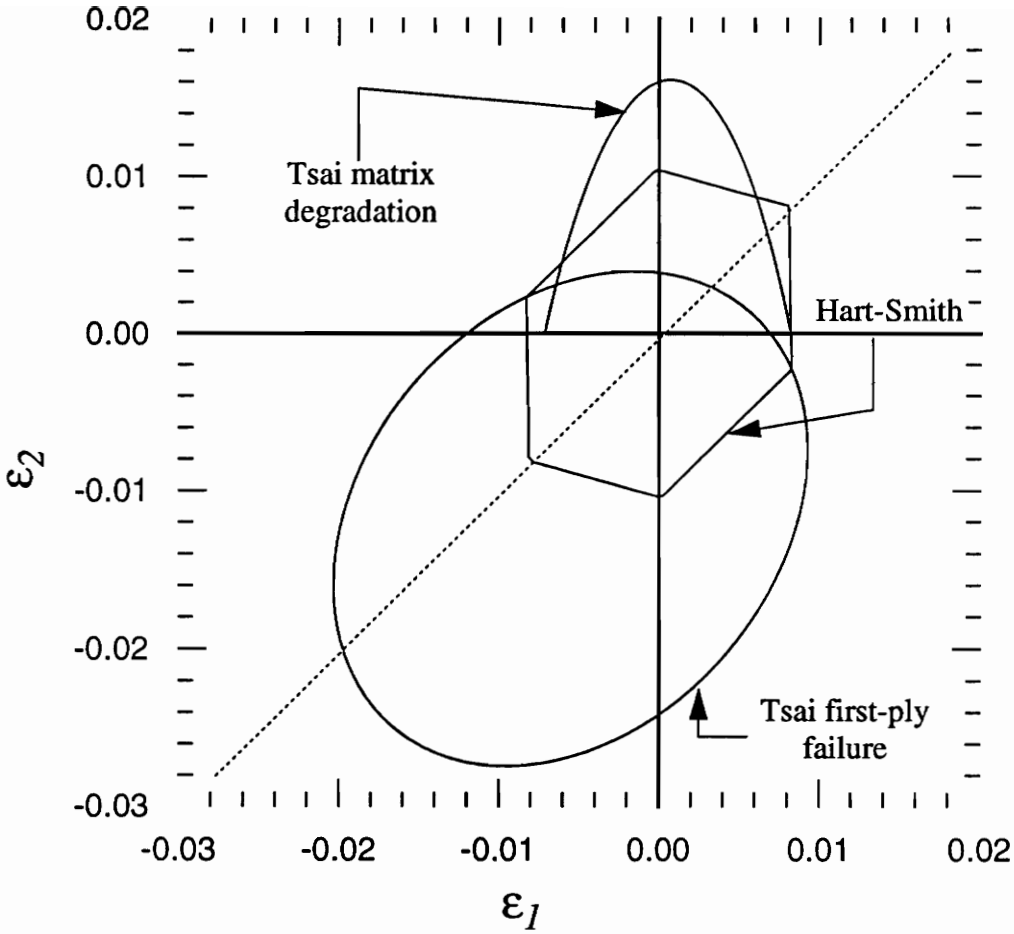

Fig. 3.1 Superimposed failure envelopes for Tsai and Hart-Smith

It would be most interesting to test the case of greatest disagreement, that of biaxial compression. It is well known, however, that compression–compression testing is very difficult, if not impossible with present technology. For this reason a test to evaluate the other case, of maximum failure load ratio, is considered instead. It is noted that the loadings all contain a dominant axial load and a smaller transverse axial load of equal or opposite sign, combined with a significant in–plane shear load. This loading type may be approximated by uniaxial loading of an off-axis specimen. In particular the fourth case in Table 3.3 is

most reminiscent of this kind of loading, and has a F value of close to the optimum. Designing a test using this simpler loading case is discussed in the next section.

3.3.3 Optimization with uniaxial loading:

An off-axis laminate loaded under uniaxial tension that is practical from the experimental perspective is now designed to maximize the predicted failure load ratio F, as defined before.

In a uniaxial test the three stress resultants are no longer independent as in the case of general loading. Denoting the load axis with X and the specimen principal fiber axes by a x-y system, the axial stress resultant N_X is related to laminate resultants to N_x, N_y, and N_{xy} through the off-axis angle Θ between X and x, as follows:

$$N_x = N_X \cos^2(\Theta)$$

$$N_y = N_X \sin^2(\Theta)$$

$$N_{xy} = -2N_X \sin(\Theta)\cos(\Theta)$$

The angle Θ has the range 0° to 22.5°, as there are always fibers at 45° to each other present. The coordinate systems used here are illustrated in Fig. 3.2. The optimization

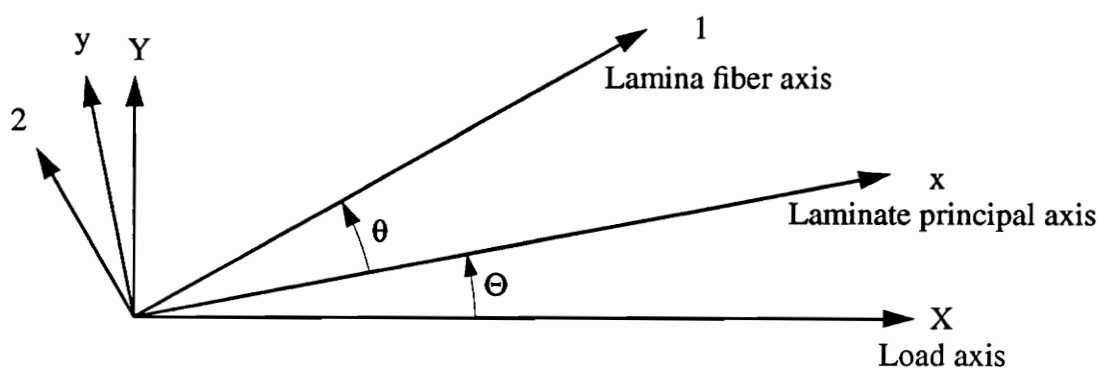

Fig. 3.2 Load-, principal laminate-, and lamina fiber-coordinate system definitions and nomenclature.

problem now reduces to finding the off-axis load angle Θ combined with the laminate giving the largest failure load ratio. For practical reasons increments of less that one degree in Θ are unreasonable, and as noted earlier only ply content, not sequence, is important. For 16-ply symmetric, balanced laminates meeting the requirements set by Hart-Smith, and using one degree increments in Θ, the design space reduces to only 207 candidates. The optimum was found by simply trying all cases. Results are presented in Fig. 3.3.

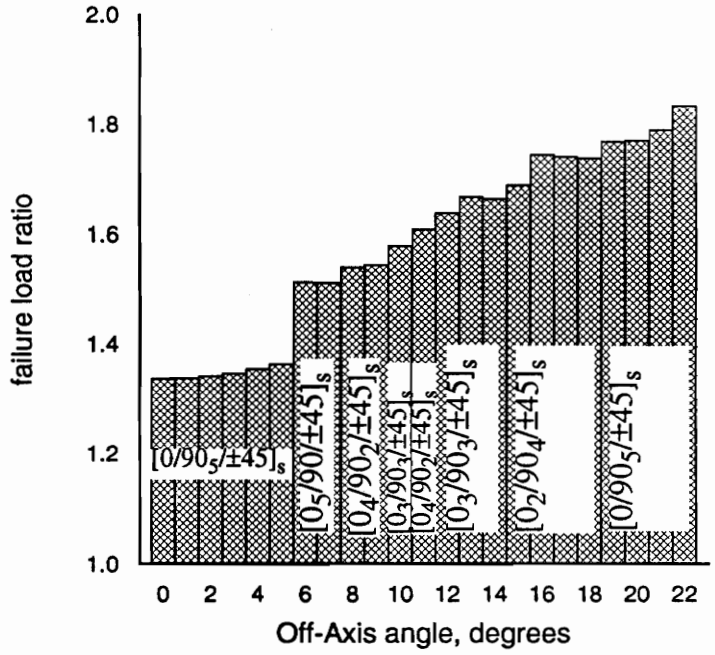

Fig. 3.3 Failure load maximization for off-axis angles of selected laminates under uniaxial tensile loading

In the Fig. 3.3 the failure load ratio F, is plotted against the off-axis angle Θ, and the laminate for which the maximum value of F is found is shown. The maximum is found at the off-axis angle 22°, with $F = 1.832$, for the laminate $[\,0 / 90_5 / \pm 45\,]_s$. As may be expected the maximum obtained in section 3.2, under general loading, of $F = 1.8897$ is not

achieved, but the difference is quite small. All the laminates in Fig. 3.2 are characterized by the fact that all contain the minimum number of ±45° plies. As the difference is in-plane shear response, this is not surprising, as the ±45° plies stiffen the laminate with respect to shear.

For testing purposes not only is the maximum difference in failure loads important, it is also important to have a specimen that is easy to manufacture, and promises good behavior under test. The laminate dominating Fig. 3.2 has five 90° plies for each 0° ply. With this laminate it will be hard to properly intersperse the layers, as required by Hart-Smith, and to limit delamination sensitivity. For this reason, the laminate appearing at 10° off-axis angle, namely $[\,0_3\,/\,90_3\,/\pm45\,]_s$ was selected for testing. This laminate has a predicted failure load ratio of 1.57854, which should be easily measurable experimentally, and is easy to intersperse properly. In addition to 10° off-axis tests the same laminate will also be tested on-axis, to compare the two criteria under simple loading. For this type of loading the failure load ratio is 1.14905.

Only the number of plies of each orientation in the laminate has been determined so far, as the stacking *sequence* has no influence on membrane response. Stacking sequence is now chosen, based on an approximate delamination analysis given by Pipes and Pagano [19]. The parameter used for delamination sensitivity comparison is the pealing stress σ_z at the laminate free edges. The pealing stress σ_z is required close to the edge due to the lack of moment equilibrium around the x-axis, caused by the free edge condition requiring σ_y to be zero at the edge. From the edge moment required to balance σ_y, σ_z can be calculated if it's distribution is known. The distribution assumed by Pipes and Pagano is shown in Fig. 3.4, and the value of σ_z is calculated for each interface in the laminate. The maximum tensile σ_z value in the laminate is taken as indicative of the the laminate's delamination sensitivity. For the laminate in question all possible stacking sequences were tried and the laminate corresponding to the smallest tensile σ_z at the free edge was selected. Consequently, the sixteen-ply laminate selected for testing has the stacking sequence of [0 / 90 / 45 / 0 / 90 / –45 / 90 / 0]s.

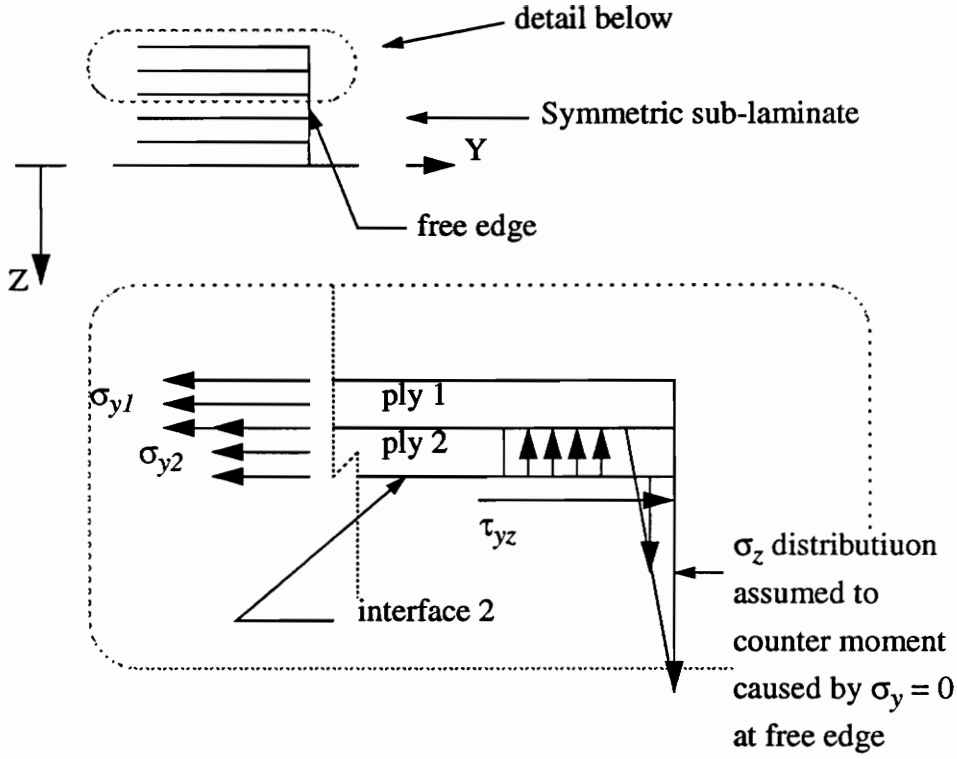

Fig. 3.4 Free body diagram of plies at free edge showing free-edge stresses needed for equilibrium.

This concludes the discussion on specimen design. The next two chapters will focus on the experiments

Chapter 4 : Experiments

Experiments were conducted on three specimen types. Unidirectional specimens loaded in the fiber direction were used to verify fiber dominated tensile properties. The laminate chosen in the optimization process, $[0 / 90 / 45 / 0 / 90 / -45 / 90 / 0]_s$, was tested both on-axis and at the selected off-axis angle of 10°. Specimen design, preparation, material used and experimental equipment and procedures are detailed in the following sections.

4.1 Material

All tests were performed on specimens made from BASF G30-500/5208 pre-impregnated unidirectional tape. A supply of this material was obtained as a gift from BASF Structural Materials, Inc. It was selected based on availability and great similarity of properties to the

T300/5208 material. In Tsai's book [5] all the necessary micromechanical and macromechanical properties of T300/5208 material are given. Since the BASF material was available and has properties very close to T300/5208 it was decided to use this material. The 5208 resin system is a thermoset epoxy while G30-500 fibers are standard modulus carbon fibers. Nominal material properties supplied by BASF for G 30-500 /5208 and the T300/5208 material systems are given in Table 4.1 for comparison and reference. The BASF material was supplied as 5.98 inch wide tape.

TABLE 4. 1 Nominal room-temperature material properties supplied by BASF Structural Materials, Inc.

Property	G30-500/ 5208	T300/5208
E_1, Msi	20.8	20.5
E_2, Msi	1.25	1.24
X, ksi	230	221
X', ksi	218	215
Y, ksi	7.5	7.6
S, ksi	11.3	11.15

4.2 Oblique tabs

In Chapter 3 the design process results in two specimens to be tested. Both have the same layup, but one is to be tested on-axis and the other under 10° off-axis loading. Due to the directional nature of composite materials off-axis coupons exhibit extension-shear coupling, giving rise to problems of gripping these coupons for testing. The problem amounts to finding physical means of providing the boundary conditions to allow the specimen to deform in the required fashion. The approach most commonly used to overcome this problem is to use long, tapered tabs. These allow the load to be introduced gradually, allowing the deformations to increase slowly within the tabbed area. Long tapered tabs are however expensive and difficult to make, and they only reduce the magnitude of the problem.

In a recent paper by Sun and Chung [23] the use of bonded, oblique tabs was introduced for uniaxial testing of off-axis specimens. The approach is based on matching contours of constant axial displacement of the specimen with the tabs, so that the homogeneous deformation field in the specimen can be matched by the boundary conditions.

For a symmetric laminate subject to a spatially uniform uniaxial tensile load N_X, the axial displacement u_0 is

$$u_o = (\bar{A}_{11}^{-1} X + \bar{A}_{16}^{-1} Y) N_X \qquad 4.1$$

in which $\bar{A}_{11}^{-1}$ and $\bar{A}_{16}^{-1}$ are the inverse components of the membrane stiffness matrix $\bar{A}$ in the X - Y coordinate directions. The coordinate systems used are shown in Fig. 4.1, with X aligned with the load axis, and x alligned with the 0° fiber axis. It can be seen that along a line at angle ψ with the X-axis, with ψ given by:

$$\cot\psi = -\frac{\bar{A}_{16}^{-1}}{\bar{A}_{11}^{-1}} \qquad 4.2$$

the X-direction axial component of displacement is maintained uniformly; i.e., lines at angle ψ are constant u_0 contours for the specimen. Rigidly supporting a test specimen along this line should overcome the problem of axial-shear coupling. In this way Sun suggests using oblique, bonded tabs on specimens loaded off-axis. Sun notes that the Poisson contraction in the Y direction cannot be accommodated using bonded tabs. This is however the case for all tabbed specimens, and is not considered an important effect. The use of oblique tabs was adopted for the off-axis specimens used here. For the 10° off-axis laminate [0 / 90 / 45 / 0 / 90 / –45 / 90 / 0]$_s$ with nominal properties as used in Chapter 3, the off axis angle was found to be given by ψ = 63.5°.

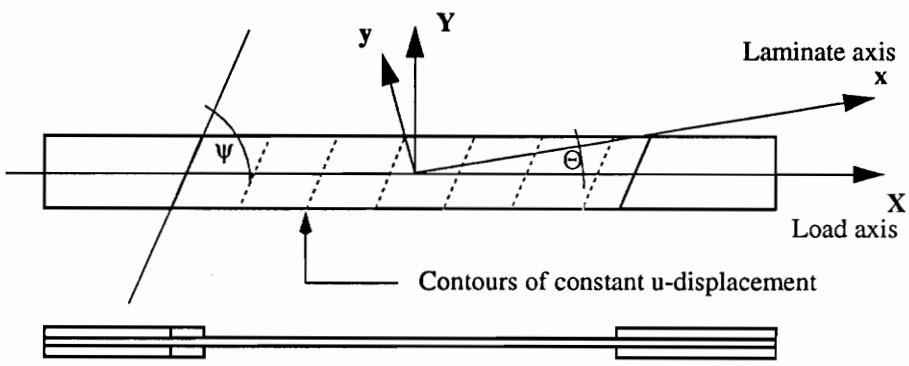

Fig. 4.1 Oblique bonded tabs.

4.3 Specimen preparation

Two 11″ by 11″ panels of the laminate [0 / 90 / 45 / 0 / 90 / –45 / 90 / 0]$_s$ and one 11″ by 11″ 8-ply unidirectional panel were manufactured from BASF G30-500 / 5208 material in a press-clave, using the manufacturer's recommended cure cycle, as shown in Fig. 4.2.

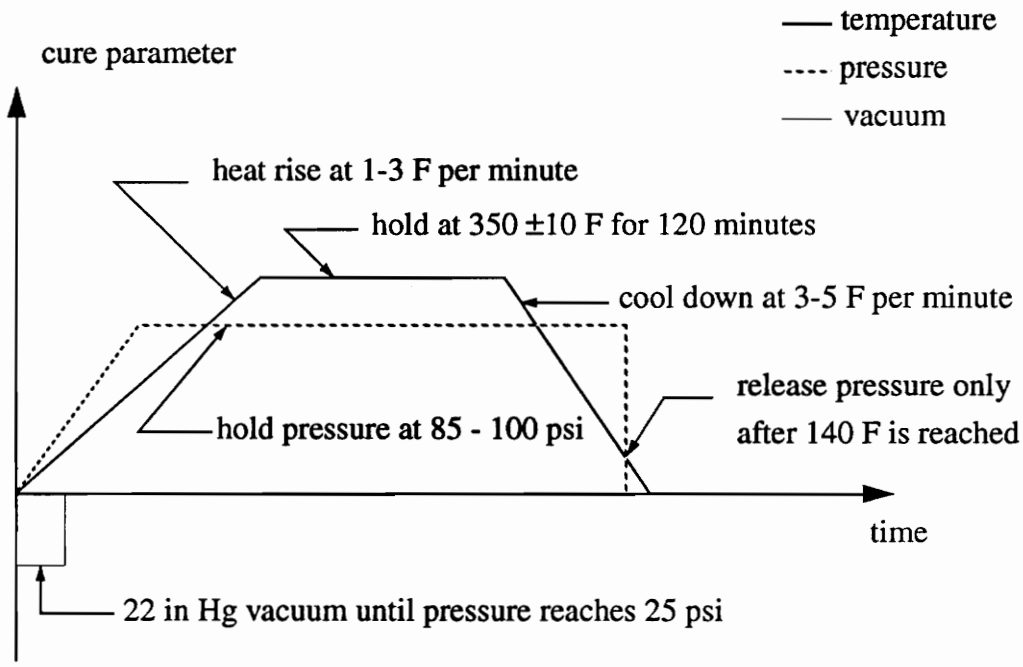

Fig. 4.2 Recommended cure cycle for BASF G30-500 / 5208.

The press-clave, see Fig. 4.3, is essentially a miniature autoclave. It is used between the platens of a hot-press which supply heat and clamping force, and uses an internal membrane to apply pressure to the panel being made. In this way small flat panels can be made economically and with better control of temperature than is possible in an autoclave. All finished panels were inspected for defects using ultrasonic C-scan. The 16-ply laminates were found to be virtually perfect, while the 8-ply unidirectional panel showed some evidence of porosity. The indicated porosity was however judged satisfactory as it is normal for such panels not to achieve complete homogeneity, due to the difficulty of extracting all voids from thin unidirectional panels. The panels were trimmed to a rectangular planform with edges parallel or perpendicular to the fiber directions.

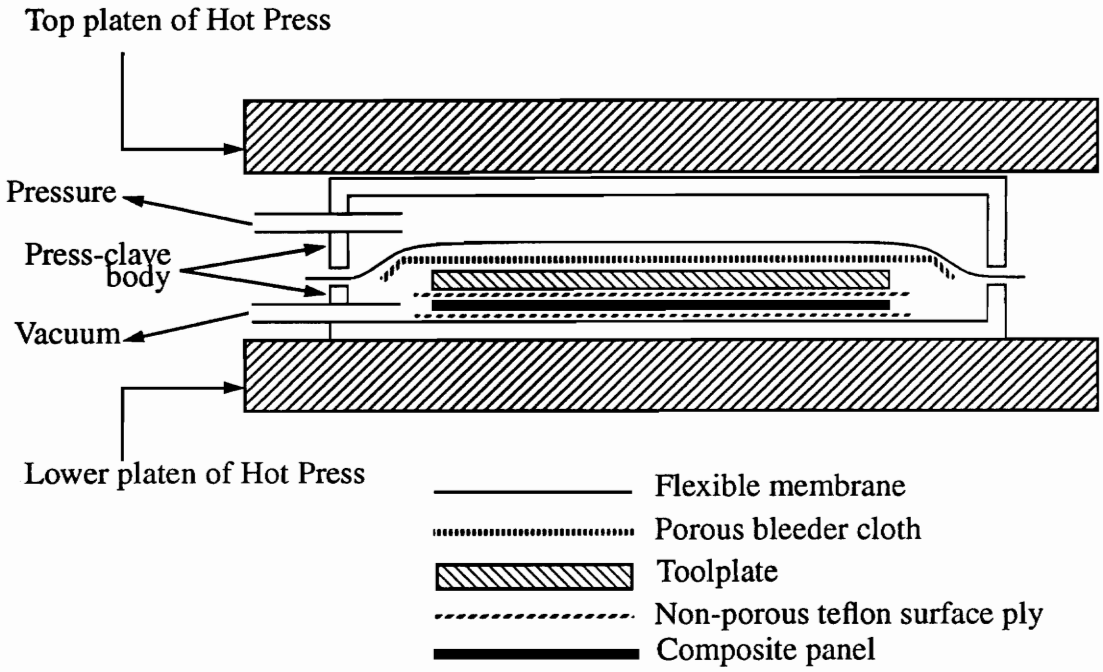

Fig. 4.3 Schematic showing characteristics of a press-clave used to manufacture flat composite panels.

Standard 3/32-inch-thick G-10 glass-epoxy tab material was used for all the specimens. The tabs were all nominally 2.4 inches long, as required for the grips of the testing machine. Tab material was bonded to the panels one side at a time so that the tab area may be ground down to the correct thickness before the other side's tabs are applied. Tab material was bonded to whole panels using 3-M DP–460 high-toughness room temperature cure epoxy. Control of the bond-line thickness was achieved by inserting lengths of 0.007″ diameter copper wire in the bondline, spaced approximately 2″ apart. All tabs had rectangular edges, with the sharp edge directly adjacent to the panel being chamfered by light sanding. Preparation for bonding was achieved by sand-blasting the tab material, lightly sanding the bonding area on the composite panels, and cleaning both surfaces with acetone. The tab material was located on the panel using a length of adhesive tape along the edge adjacent to the specimen gage section. This tape also served as a "mold" to form a fillet of adhesive to smooth the transition between the tab and specimen. Tab material was bonded onto the panels using a toolplate and small aluminum rectangles to locate the tab relative to the panel, and the tab material uniformly pressed into the 3-M adhesive using a second toolplate. No vacuum bagging or high temperature cure was used, the adhesive was

simply allowed to cure under ambient pressure and temperature. After the first side of a panel was tabbed and ground this was repeated for the other side, giving a final thickness in the tab area of 0.250″ ±0.002″ as required for the hydraulic grips used (MTS Model 646.25). For the off-axis specimens the tab material was applied in two sawtooth-pattern pieces per side, so as to achieve a longer gage length.

Specimen dimensions were based on ASTM standard D 3039. The unidirectional specimens were 0.5″ wide with a 6.0″ gage section, and 2.4″ tabs. Both the on-axis and 10° off-axis specimens were 1.0″ wide, with gage section lengths of 6.0″ and 5.5″, respectively, and 2.4″ nominal tabs, (see Fig 4.4). After tabbing, the on-axis and 10° off-axis specimens were cut from the panels slightly oversize using a diamond-bladed bandsaw. The edges were then precision ground using a diamond dressing stone to achieve the final width. Due to manufacturing delays, the unidirectional specimens were cut from the panels using a diamond-bladed circular saw, and the edges sanded smooth on a flat surface. All the specimens were numbered, measured using a micrometer, and dimensions were recorded The dimensions of the specimens are shown in Tables 4.2, 4.3, and 4.4 for the unidirectional, on-axis, and off-axis specimens, respectively, with the measurement positions shown in the adjacent illustrations. The unidirectional specimens had slightly more variation in the width than the other specimens, hence the two width measurements. Likewise, the thicker on-axis and 10° off-axis specimens had larger thickness variations than the unidirectional specimens, so three thickness measurements were taken. The unidirectional specimens were labeled UD1 through UD8, the on-axis specimens as A1-A8, and the off-axis specimens as B1-B6.

From *areal fiber weight*, defined as the mass of dry fibers per unit planform area of prepreg material, resin volume fraction, nominal, as-cured ply thickness, and fiber specific gravity, all supplied by the manufacturer, and thickness measurements of the finished panels, the fiber volume fraction v_f of finished panels were calculated as 0.7 ± 1% for all three panels. The areal fiber weight supplied was 132 grams (metric) per square meter of prepreg, the resin volume fraction 32% and fiber specific gravity was 1.75. The nominal, as-cured ply thickness was suplied as 0.0055″.

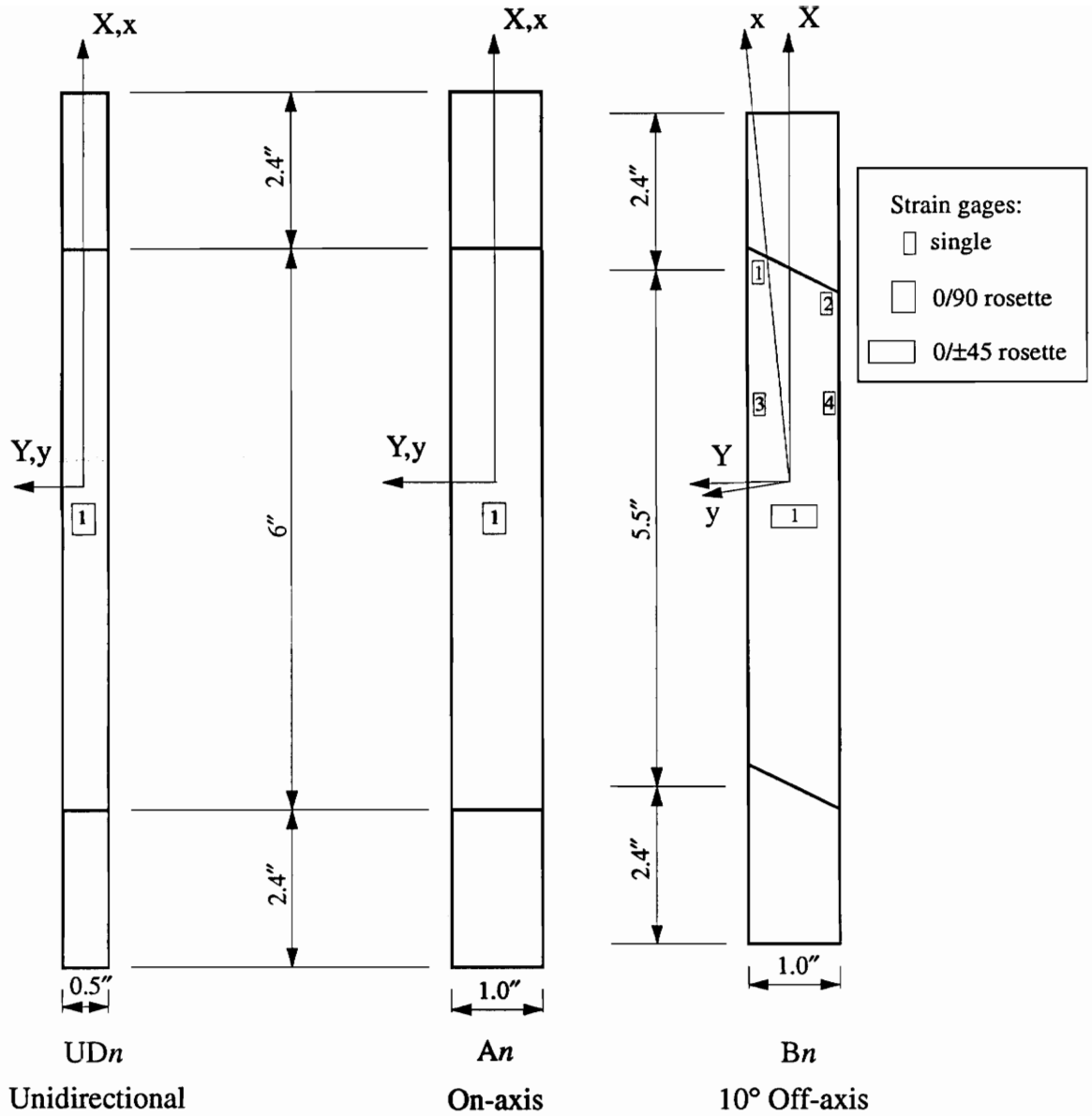

Fig. 4.4 Nominal specimen dimensions, position and numbering of strain gages

TABLE 4.2 Unidirectional 8-ply specimen dimensions

Specimen	w1	w2	t
		inch	
UD1	0.5255	0.5253	0.0416
UD2	0.5287	0.5290	0.0418
UD3	0.5330	0.5300	0.0415
UD4	0.5270	0.5270	0.0422
UD5	0.5300	0.5330	0.0416
UD6	0.5310	0.5290	0.0420
UD7	0.5290	0.5290	0.0420
UD8	0.5300	0.5290	0.0418
Average width	0.5290 inch	Average thickness	0.04182 inch

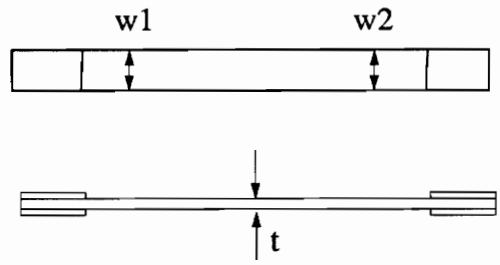

TABLE 4.3 16–Ply on-axis specimen dimensions

Specimen	t1	t2	t3	w
			inch.	
A1	0.0829	.0.830	0.0826	1.002
A2	0.0830	0.0836	0.0834	1.0015
A3	0.0834	0.0836	0.0839	1.001
A4	0.0830	0.0890	0.0838	1.001
A5	0.0839	0.0831	0.0841	1.001
A6	0.0839	0.0843	0.0838	1.000
A7	0.0838	0.0842	0.0838	1.000
A8	0.0831	0.0837	0.0836	1.000
Average thickness	0.08377 inch		Average width	1.0008

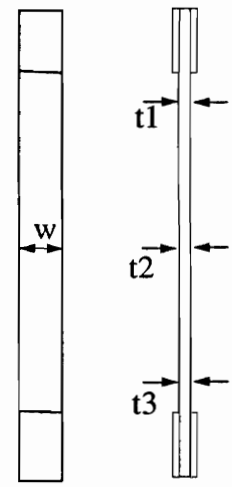

TABLE 4.4 16-Ply 10° off-axis specimen dimensions.

Specimen	t1	t2	t3	w
			inch.	
B1	0.0844	0.0837	0.0840	1.0005
B2	0.0848	0.0856	0.0855	0.9975
B3	0.0848	0.0844	0.0841	1.0005
B4	0.0848	0.0848	0.0851	0.9980
B5	0.0847	0.0851	0.0852	1.0000
B6	0.0843	0.0841	0.0839	1.0005
Average thickness	0.08461		Average width	0.9995

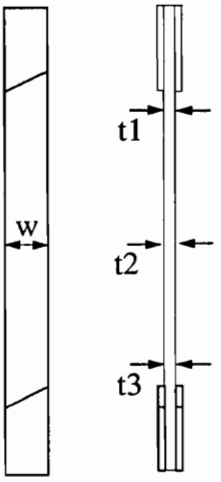

4.4 Test equipment and instrumentation.

Experiments were performed using a MTS servo-hydraulic testing system. This system is comprised of a Model 319.5 axial-torsional load unit, equipped with Model 646.25 hydraulic grips. Control of the system is either directly from a Model 458.20 Micro-Console, with associated AC and DC controllers and a function generator, or from a DEC Model PDP 11/53 Mini-Computer, interfaced through a MTS Model 468.01 interface, providing computer control of the test and simultaneous data acquisition. Axial and torsional capacity of the frame is 100,000 lb. axial and 50,000 lbs-in. torsional loading, respectively. The Model 646.25 hydraulic grips accept gripping collets for either round specimens or flat specimens of different thicknesses. For each set of collets precise control of specimen thickness or radius is essential, with thickness tolerances in the gripping area of the specimen of typically ±0.002″. The grips are however then guaranteed to provide correct alignment of a specimen. Gripping pressure of these hydraulic grips can be set to suit the type of tests. In all cases the grip supply pressure was set to approximately 2000 psi.

The tests were controlled in all cases from the Micro-Computer. Data channels sampled were for axial load and displacement, torque and rotation, and a number of strain gage

channels, up to seven (7) in total. The load and displacement information was acquired directly from the machine's internal load, torque, displacement and rotation transducers, which have been recently calibrated by a company representative. Strain information was sampled using Micro-Measurements (MM) CEA-06-125-XX-350 strain gages, used in quarter bridge configuration with a three leadwire arrangement, and a set of MM 2120A strain gage conditioners. Strain gage excitation voltage was set to three (3) volts, and calibration was done using internal shunt resistances in the MM 2120 A conditioning units, taking account of individual gage factors, and automatically compensating for leadwire resistance. The MTS Model 468.01 interface requires input signals of ± 10 volts, consequently the gain on the MM 2120A conditioners were adjusted to provide $\frac{2}{3}$ volt / 1000$\mu\varepsilon$, thus allowing for ± 15,000 $\mu\varepsilon$ to be represented by ± 10 volt. Strain gage leadwires were connected to the MM 2120A strain gage conditioners through a set of push-pin connectors adjacent to the grips, and hardwired to the conditioners.

Both the unidirectional specimens,UD1-UD8, and on-axis specimens, A1-A8, were strain gaged by a single 0°/90° MM CEA-06-125-UT-350 gage, with -125- referring to the 0.125″ gage length of these gages, bonded to the center of the test section. The off-axis specimens, B1-B6, were instrumented by a single MM CEA-06-125-UR-350 rosette in the center of the gage section. In addition specimen B1 and was instrumented more completely to check the uniformity of the strain field produced. In Sun and Chung's paper their specimens are instrumented with axial gages close to the oblique tabs on both sides of the specimen to check for an in-plane moment that would result from the oblique tabs failing to supply the appropriate boundary conditions. This was repeated on specimen B1 using two MM CEA-06-125-UN-350 gages. In addition axial gages were applied away from the tabs, recording the gage section axial strain to check for uniformity and comparison to the strains measured at the tabs. The location of strain gages are shown in Fig. 4. 4 and Fig. 4.5.

4.5 Procedures

During testing the following procedures were followed. The specimens were inserted in the hydraulic grips, with the complete tabbed area in contact with the collets. One side of the specimen was gripped and the strain gage leads connected to the conditioner inputs.

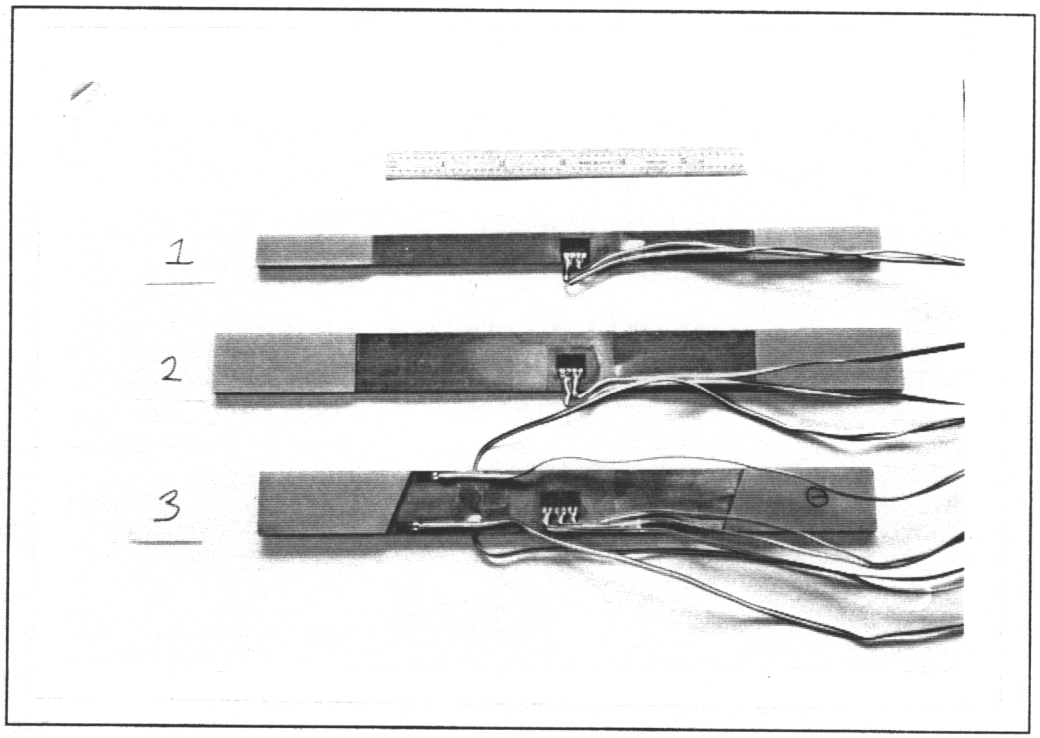

Fig. 4.5 Photograph showing position of strain gages on final specimens.

All gages were then calibrated, the gain adjusted, and the bridge balanced, as described in section 4.4, before the specimen was gripped at the other end. The axial actuator was controlled in displacement for all tests, with displacement rate set to achieve approximately 1% strain per minute. Test parameters such as number of channels sampled, loading rate, data file names, etc., were entered into the test computer, and the test started. During testing the specimen were observed closely, from behind a transparent screen. Any premature failures, delaminations or uneven failures observed were recorded, and used to judge the quality of the test.

Results of experiments, photographs of failed specimens, and description of failures are given in chapter 5.

Chapter 5 : Experimental Results and Discussion

In this chapter details and results of experiments and comparison with predictions are presented and discussed. Experiments on unidirectional specimens are discussed first, and material properties used in the final analytical predictions are then established. The predicted failure loads for on-axis and 10° off-axis tests are reported. The results of on-axis tests and 10° off-axis tests are presented next, with details of failure loads, stress-strain information, etc., compared to theory. Experimental results and comparisons are then discussed, conclusions drawn, and suggestions for future work are given.

5.1 Unidirectional specimens and measured material properties

Eight unidirectional specimens as described in chapter 4, Fig. 4.4, with dimensions recorded in Table 4.2, were tested to failure under axial tension. During testing, longitudinal and transverse strains, and axial load, were recorded in 0.5 second increments over the 100 second duration of the tests. Loading was under displacement control, with a constant cross-head speed set to achieve approximately 1% strain per minute. Of the eight specimens tested, UD1-UD8, two failed in a manner considered unrepresentative, with the failure clearly initiating at one side of the specimen at considerably less than the average failure load, and the specimen "tearing" from one side to the other. These specimens, UD3 and UD8, were withdrawn from consideration. Failure in the other specimens was typically initiated by longitudinal splits forming through the length of the specimen, parallel to the fibers, and normally closer to one side than the other, followed by a sudden, dramatic explosion of the specimen. A photograph of a failed specimen is given in Fig. 5.1, demonstrating the violent nature of failure. Judging whether the failure occurred in the gage section was virtually impossible due to the violent nature of the event. As noted, however, some specimens did not fail in this dramatic fashion and these were judged to have failed in a manner inconsistent with fiber-strength dominated failure.

Three mechanical properties of the material are extracted from the measured data. These are fiber direction modulus E_1, fiber direction tensile strength X, and Poisson's ratio, ν_{12}. Specimen modulus and Poisson's ratio are calculated from the average cross-sectional area and the stress and strain at 66% of failure load. A least squares fit of the stress-strain data could also be employed, but since the stress-strain plots were quite linear, see Fig. 5.2, this was judged unnecessary. The measured moduli and Poisson's ratios are given in Tables 5.1 and 5.2.

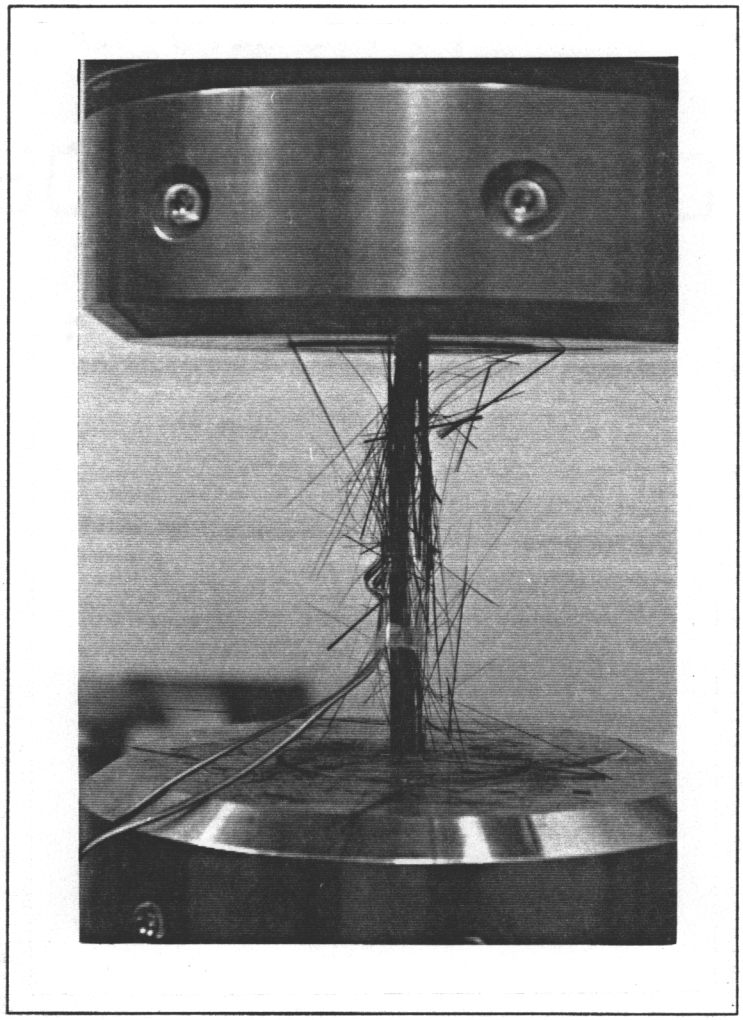

Fig. 5.1 Photograph showing failed unidirectional specimen.

TABLE 5.1 Fiber direction modulus for the unidirectional specimens. Strain and load reported at approximately 66% of the failure load.

Specimen	Average area square in.	Load lb.	Stress ksi	Strain %	E_1 Msi
UD1	0.02186	4032.7	184.51	0.8564	21.54
UD2	0.02211	4116.4	186.21	0.8394	22.18
UD4	0.02224	4077.9	183.37	0.8233	22.27
UD5	0.02211	4059.6	183.61	0.8665	21.19
UD6	0.02226	4013.2	180.29	0.7965	22.64
UD7	0.02222	4042.1	181.97	0.8114	22.43
				Average	22.04 Msi
				C.O.V.	2.5%

TABLE 5.2 Poisson's ratios from unidirectional specimens. Strains reported at approximately 66% of the failure load.

Specimen	ε_1, %	ε_2, %	ν_{12}
UD1	0.8564	-0.2371	0.2768
UD2	0.8394	-0.2376	0.2831
UD4	0.8233	-0.2449	0.2975
UD5	0.8665	-0.2572	0.2968
UD6	0.7965	-0.2255	0.2831
UD7	0.8114	-0.2262	0.2788
		Average	0.2860
		C.O.V.	3.1%

Fiber direction tensile strength is calculated from the largest load recorded and the minimum measured cross-sectional area. Results are presented in Table 5.3.

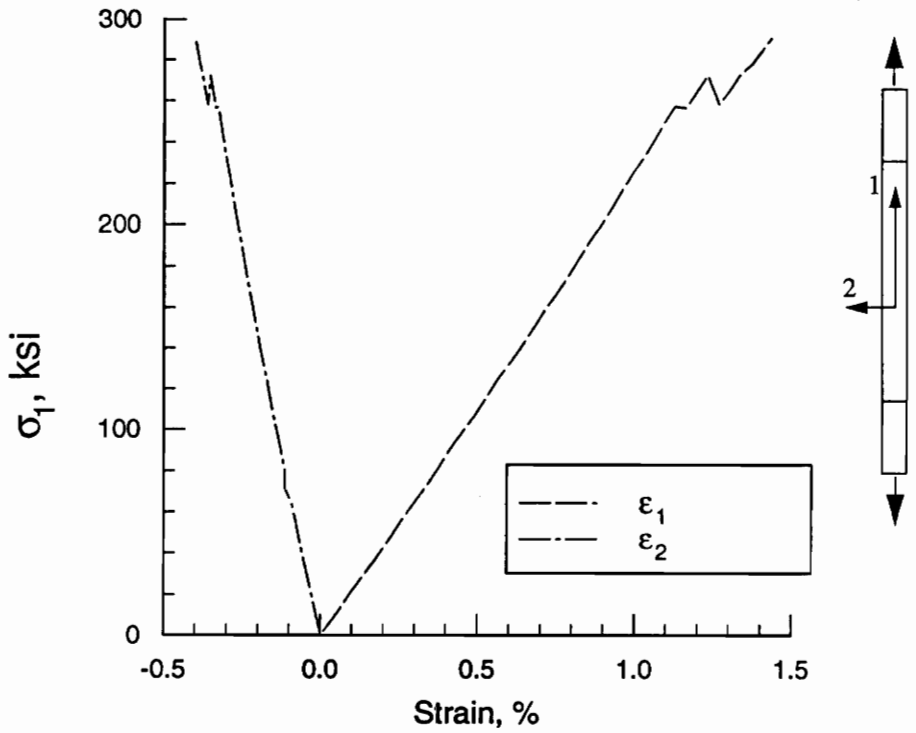

Fig. 5.2 Stress vs. axial strain, ε_1, and transverse strain, ε_2, from unidirectional specimen UD4.

TABLE 5.3 Fiber direction strengths of the unidirectional specimens.

Specimen	Minimum Area square in.	Failure Load lb.	Failure Stress ksi
UD1	0.02185	6719.0	307.51
UD2	0.02210	6687.0	302.58
UD4	0.02224	6643.9	298.74
UD5	0.02205	6333.7	287.24
UD6	0.02222	6387.4	287.46
UD7	0.02222	6366.0	286.50
		Average	295.01 ksi
		C.O.V	3.1%

The three quantities measured are compared to published data in Table 5.4. Note that supplier's data is adjusted where needed for the fiber volume fraction, v_f, of the specimens tested. As noted in chapter 4, all specimens had a fiber volume fraction of 0.7 ± 1%.

TABLE 5.4 Comparison of published and measured properties determined from unidirectional specimens.

Property	Measured	Published	Difference, %	Source of published property.
E_1, Msi	22.04	22.40	-1.6	supplier, adjusted to $v_f = 0.7$
X, ksi	295.01	247.69	+19.1	supplier, adjusted to $v_f = 0.7$
ν_{12}	0.286	0.28	+2.1	Tsai, T300/5208, [5]

Modulus E_1 is very close to the published value, being 1.6% lower. Poisson's ratio is not quite as close, at 2.1% high, but still not very different. Tensile strength, X, is however 19.1% higher than the published value, not an insignificant difference. Discussions with the supplier, however, revealed that the published axial strength values are quite conservative. The strengths measured in the tests are considered normal by the supplier, and the fairly low coefficient of variation of 3.1% tends to bear this out. The measured values are accepted as reported.

The final set of material properties used in analytical predictions are now established. Material properties are obtained from three sources. The fiber dominated tensile properties were measured directly, as described and reported in Table 5.4. Other properties are taken from manufacturer data sheets, and these are given in Table 5.5. Properties not available from these sources are taken from literature; see Table 5.6. The material used, BASF G30-500 graphite fibers in 5208 epoxy resin, is very similar to the widely used T300-5208, and in some cases it is necessary to assume properties are the same. Where necessary, properties are adjusted to account for volume fraction. For the final value of E_2, micromechanics equation 2.10, described in chapter 2 and found in [5] is used. In addition, Tsai's assumptions, [5, p. 7-15], that transverse compressive strength, Y', and shear strength, S, does not vary for small changes in v_f are used in accepting BASF values at $v_f = 0.65$ for these properties. The source and values of the different properties for $v_f = 0.7$ are presented in Table 5.7.

TABLE 5.5 Supplier data: BASF Structural Materials, Inc.

Property	Value	v_f	Comments
E_1, Msi	20.8	0.65	
E_2, Msi	1.25	0.65	
E_m, Msi	0.546	n/a	
X, ksi	230.0	0.65	
X', ksi	218.0	0.65	
Y, ksi	7.5	0.65	
S, ksi	11.3	0.65	Taken as 1/2 of ±45° specimen tensile strength.

TABLE 5.6 Properties from literature

Property	Value	v_f	Source
G_{12}, Msi	1.04	0.7	[5]
Y', Msi	35.67	0.7	[5]

TABLE 5.7 Final material properties, adjusted to v_f = 0.7 where needed.

Property	Value	Source	Comments
E_1, Msi	22.04	Measured	
E_2, Msi	1.322	BASF	published for v_f = 0.65, adjusted to v_f = 0.7
G_{12}, Msi	1.04	[5]	Assumed same as T300 in same matrix
ν_{12}	0.286	Measured	
X, ksi	295.01	Measured	
X', ksi	295.01	See comment	Assumed $X' = X$, common for T300, [5]
Y, ksi	7.5	BASF	No change from v_f = 0.65, [5]
Y', ksi	35.67	[5]	Assumed same as T300 in same matrix
S, ksi	11.3	BASF	No change from v_f = 0.65, [5]
E_m, Msi	0.5461	BASF	
G_m, Msi	0.2022	Calculated	From E_m, ν_m = 0.35, typical, [5]

5.2 Analytical predictions and experimental results for on-axis specimens.

In Chapter 3 optimal specimens were designed based on nominal material properties found in [5], and ignoring hygro-thermal effects. Material properties listed in Table 5.7 were used to reanalyze the optimal laminate, $[\,0\,/\,90\,/\,45\,/\,0\,/\,90\,/\,-45\,/\,90\,/\,0\,]_s$, for on-axis tests, to find failure predictions based on these new properties. Hygro-thermal effects were included where reasonable. During discussions the author had with Dr. Hart-Smith the latter stated that for his criterion no hygro-thermal effects should be used, as it is a fiber failure model and hygro-thermal effects affect mainly the matrix. Tsai, on the other hand, advocates the inclusion of both the effect of temperature change between the elevated cure temperature and operating temperature, and the effect of moisture absorption. In Tsai's commercial codes little provision is made for not using both the effects of temperature difference and 0.5% moisture content (by mass), short of changing the material properties file.

The predictions including both temperature and moisture effects are considered most representative of Tsai's model and will be used here in the discussions of failure load ratios. For completeness, however, the predictions of Tsai's criterion for the cases of no hygro-thermal effects, and temperature effects only, are also presented.

Failure prediction with Hart-Smith's criterion results in prediction of a single failure load that produces failure in a single ply or family of plies (such as ±45°). Tsai predicts a series of failure loads and corresponding plies, from first-ply failure to last-ply failure. The predictions are presented in Table 5.8. Note the effect of the different approaches to hygro-thermal effects on Tsai's predictions. In the case of both temperature and moisture these effects can be seen to counteract each other, producing failure prediction close to the case of no hygro-thermal effects. Although Tsai predicts a series of ply failures, the critical ply is the same for the two theories, and the failure loads are quite close.

Eight on-axis specimens, labeled A1 to A8, as described in chapter 4, Fig. 4.4, with dimensions recorded in Table 4.2, were tested under axial tension to failure. Longitudinal and transverse strains, and axial load, were recorded in 0.5 second increments over the 100 second duration of the tests. Loading was under displacement control, with a constant cross-head speed set to achieve approximately 1% strain per minute.

TABLE 5.8 Failure predictions for 16-ply on-axis specimens; calculated for final material properties and hygro-thermal effects as indicated.

Theory	Hygro-thermal	failure sequence	critical plies	failure stress, ksi
Hart-Smith	none	only one failure	0°	138.28
Tsai	none	first	90°	59.675
		second	± 45°	63.594
		final	0°	120.682
	Temperature only:	first	90°	37.887
	–180 F	second	± 45°	46.314
		final	0°	104.136
	Temp. and moisture:	first	90°	66.961
	–180 F and 0.5% H_2O	second	± 45°	68.484
		final	0°	124.48

No damage or failure initiation could be observed before final, explosive failure. During preparation for testing specimen A4 was inadvertently loaded to 10,000 lbs. and the load released. When subsequently reloaded to failure the failure load was significantly below the average, and this result was withdrawn from consideration.

A typical failed specimen is shown in Fig. 5.3. Fracture surfaces typically formed more or less directly across the 0° fiber direction and seems consistent with final failure in the 0° plies, as predicted by both theories. Failure loads and failure stresses are presented in Table 5.9.

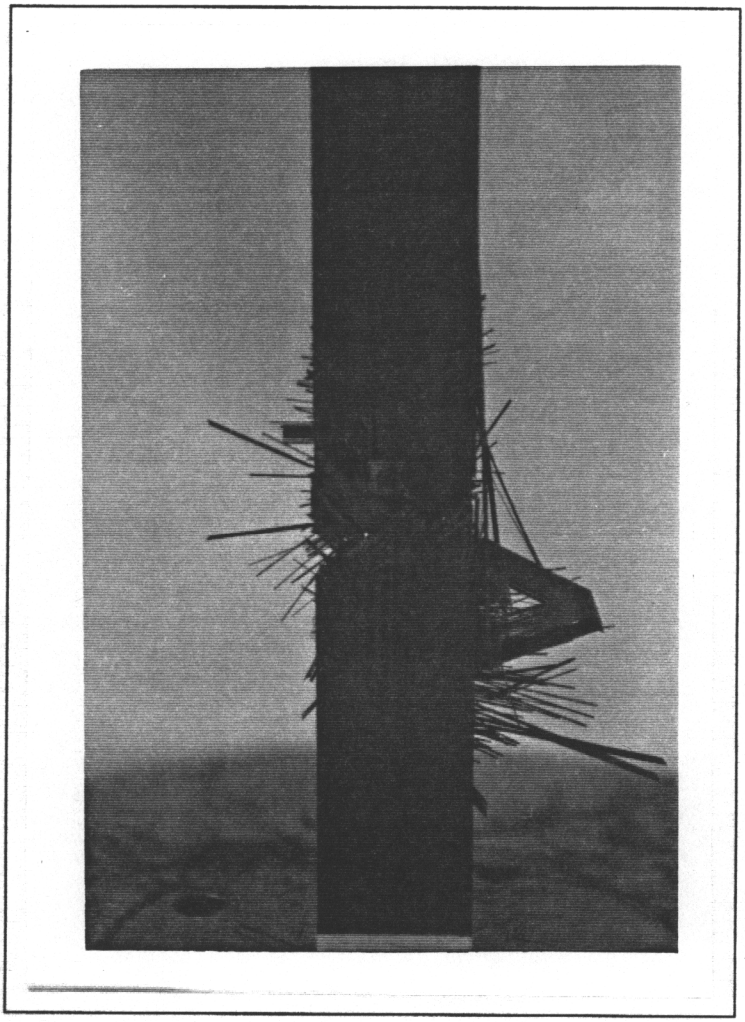

Fig. 5.3 Photograph of typical failed on-axis specimen

TABLE 5.9 On-Axis specimen strengths

Specimen	Minimum Area	Failure Load	Failure Stress
	sq. inch	lb.	ksi
A1	0.08277	11043.6	133.43
A2	0.08312	11367.2	136.76
A3	0.08348	11465.6	137.35
A5	0.08318	11370.3	136.70
A6	0.08380	11774.5	140.51
A7	0.08380	11200.5	133.66
A8	0.08310	11063.1	133.13
		Average	135.93 ksi
		C.O.V.	2.0%

Comparison of experimental results with predicted last-ply failure is given in Table 5.10.

TABLE 5.10 Experimental and predicted failure loads

Method	Failure load	Difference from experiment	Comments
	ksi	%	
Experiment	**135.93**	n/a	7 specimens, C.O.V=2.0%
Hart-Smith	**138.28**	**+1.73**	
Tsai, temp. and moisture	**124.48**	**-8.42**	Hygro-thermal as favored by Tsai.
Tsai, no hygro-thermal	120.68	-11.22	
Tsai, temperature incl.	104.14	-23.39	

Hart-Smith's prediction is virtually identical with the measured value, with Tsai including both temperature and moisture effects slightly conservative, at -8.42% lower than measured.

The measured stress-strain response for specimen A5 is shown in Fig 5.4, together with predictions, with both temperature and moisture effects included in Tsai's prediction. The measured initial modulus agrees very well with predictions. As noted before, both criteria predict final failure in the 0° plies, with Tsai predicting matrix failures in the 90° and ±45°

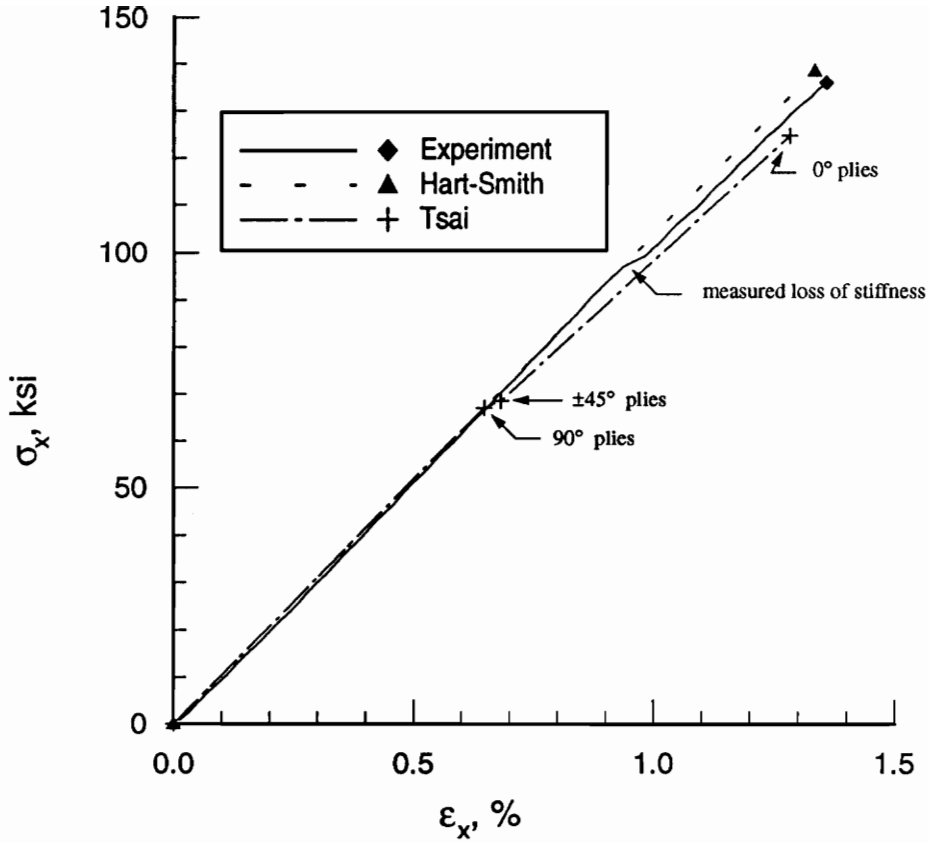

Fig. 5.4 Stress-strain curves to failure for Hart-Smith and Tsai predictions, and from the experiment on specimen A5

plies preceding final failure, and resulting in decreased modulus before final failure. The failure events modeled by Tsai are indicated by the arrows, and a measured loss of modulus also indicated. It is interesting to observe that although Hart-Smith's failure load prediction is the most accurate, the loss of modulus predicted by Tsai does seem to occur, though not quite as predicted. The measured modulus loss occurs at a higher load level, and produces a smaller decrease in modulus than for Tsai's predictions. The same loss of modulus is observed for the other specimens. The stress-strain paths for specimens A5 and A6 are shown for comparison in Fig. 5.5. It is clear that the response is very similar. For both specimens a loss of modulus can be seen at very similar load levels. The initial modulus, and modulus after the change is also very similar.

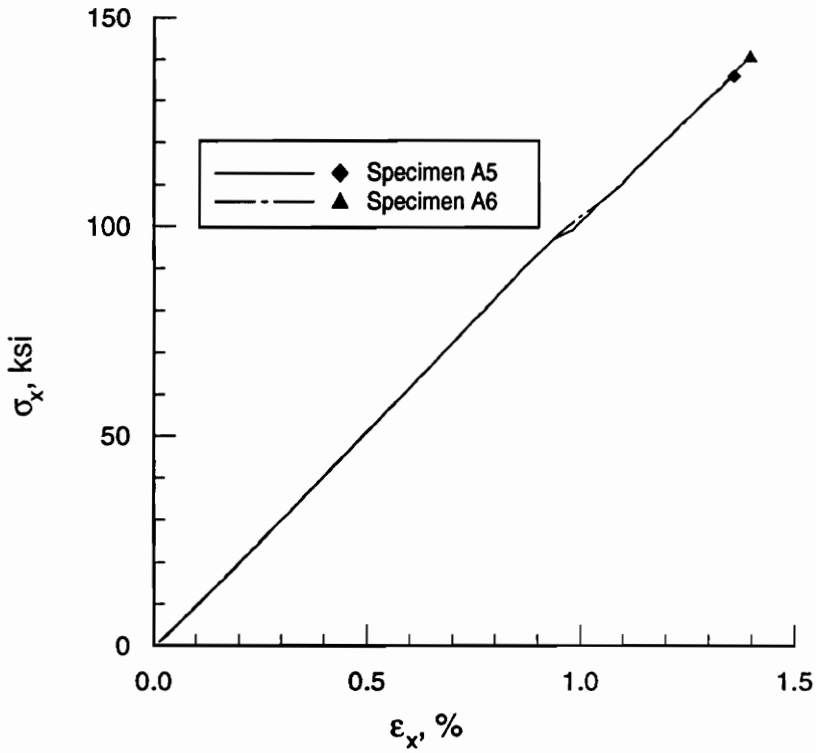

Fig. 5.5 Stress-strain path for specimens A5 and A6, demonstrating similar response

Transverse strains were also recorded. These are presented as Fig. 5.6, with $-\varepsilon_y$ plotted against ε_x, for specimen A5, and both predictions. The slope, representing the coupon Poisson's ratio, is initially the same for predictions and theory. The experimental plot then diverges from the theoretical one, with increasing Poisson's ratio, or more transverse compressive strain per axial strain. The experimental curve eventually drops off again, with all three curves ending very close together. Tsai's criterion again models a change in behavior for matrix failures, here visible as a sharp decrease in the Poisson's ratio. The drop does not, however, model the actual stress-strain path very well, occurring at too low a strain level, while the actual curve is still steepening.

Only the curves for specimen A5 is presented, as the same behavior was observed for the other specimens.

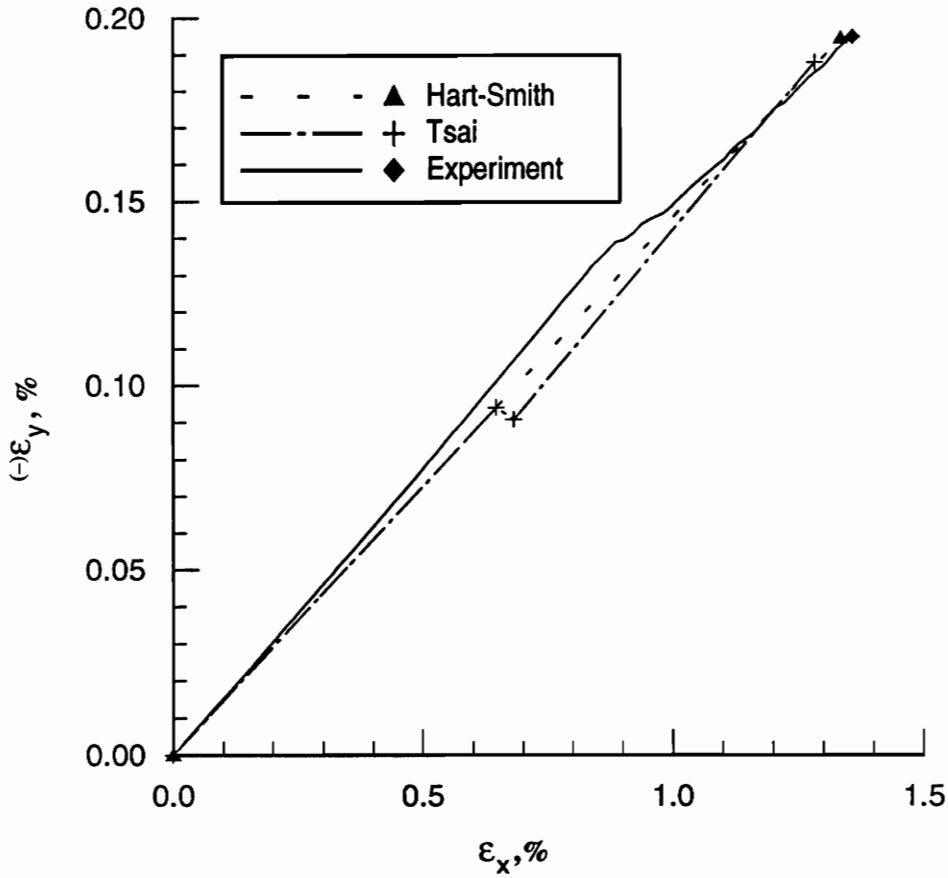

Fig. 5.6 Strains ε_x vs. ε_y for specimen A5, and both Hart-Smith and Tsai predictions.

From on-axis tests it is concluded that although Hart-Smith predicts the failure load more accurately, and Tsai models the stress-strain behavior better, there is very little significant difference between the criteria for the simple load case under consideration. Both theories model the observed response very well.

5.3 Analytical predictions of failure for the 10° off-axis specimens.

As in section 5.2, the failure load predictions for the two criteria were recalculated, using the final set of material properties, and using hygro-thermal effects as needed. The same laminate, $[\,0/90/45/0/90/-45/90/0\,]_s$ was tested on axis, as described in section 5.2

and 10° off-axis, and described in section 5.5. Failure load predictions for Hart-Smith and Tsai's criteria, for the same combinations of hygro-thermal effects used previously, are reported in Table 5.11.

TABLE 5.11 Failure predictions for 16-ply off-axis specimens; calculated for final material properties and hygro-thermal effects as indicated.

Theory	Hygro-thermal	failure sequence	critical plies	stress, ksi
Hart-Smith	none	only one failure	10°	143.15
Tsai	none	first	100°	53.90
		second	55°	50.76
		final	-35°	74.27
	Temperature only: –180 F	first	100°	35.759
		second	55°	34.16
		final	-35°	60.64
	Temp. and moisture: –180 F and 0.5% H_2O	first	100°	59.17
		second	55°	58.68
		final	-35°	77.74

Once again intermediate ply failures are reported but here the ply angles with respect to the load axis are reported, to avoid confusion between 45° and –45° plies; i.e. 55° refers to the 45° plies rotated 10°, etc. Tsai's sequence of ply failures is now different from the on-axis load case, with final failure predicted to occur in the - 35° ply. The 10° ply is still critical in Hart-Smith's prediction, as in the on-axis case.

The different approaches to hygro-thermal effects again produces a significant influence on the predictions of Tsai's model. The most impressive difference between the predictions is however the difference between Hart-Smith and Tsai's predictions. Taking Tsai with hygro-thermal effects, the objective function, F, as defined in chapter 3, is equal to 1.84. For the case of no hygro-thermal effects, the ratio $F = 1.93$ is found.

In chapter 3 for the same laminate and load case, and no hygro-thermal effects, the value $F = 1.58$ was found, but there nominal properties found in [5], were used in the prediction.

The large difference when using the new properties can be explained by calculating the sensitivities of the failure load ratio, F, to the material properties. The effect of changed properties on F is shown in Table 5.12.

TABLE 5.12 Sensitivities of objective function F to change in material properties, and predicted change in F for actual material property changes.

Property	Logarithmic derrivative of F wrt. property	% change in property from [5] to Table 5.7.	% change in F predicted
E_1	-0.60	-16	9.6
E_2	0.15	-11	1.65
ν_{12}	0.18	2	0.36
X, X'^a	0.60	35.63	21.38
Y	-0.125	29.3	-3.66
S	-0.47	14.6	-6.86

a $X = X'$ assumed

The sum of the predicted changes in F is 22.53%, which is very close to the actual change in F of 21.2%. The largest derrivatives of F with respect to properties are for E_1, X, and S.

Fortunately, the final properties yield a larger ratio, which should be easily measurable.

5.4 Influence of oblique end tabs on the response of the 10° off-axis specimens.

The efficiency of the oblique tabs was investigated by monitoring strains at opposite edges of the specimen close to the tabs, and also in the gage section, as was illustrated in Fig. 4.4. The strains recorded are plotted in Fig. 5.7, with the relative position and numbering of the gages repeated. Gages 1 and 2 are close to the tab, and gages 3 and 4 are located in the gage section, as shown. It is clear that the strains are virtually indistinguishable. Thus, the oblique tab design results in a spatially uniform in-plane strain field in the specimens. If the oblique tabs were not able to compensate for the effect of extension-shear coupling, then the gages at opposite sides of the specimen close to the tabs would register different strains, as the rigid boundary conditions imposed by the grips would cause an in-plane bending moment. The placement of the gages to examine the spatial uniformity of the

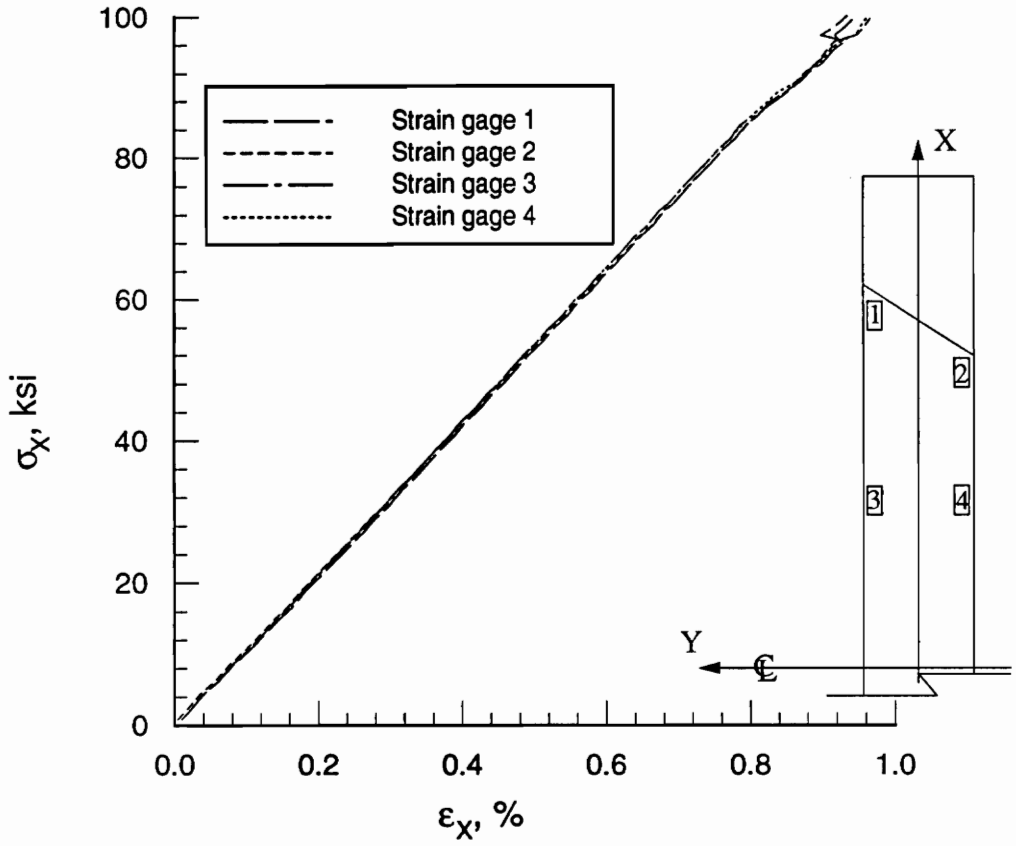

Fig. 5.7 Axial strain gages 1 to 4, recording the axial strain field in specimen B1.

response is the same as used by Sun and Chung [23]. The uniformity of the strains in the present off-axis tests are similar to what Sun and Chung found in their tests.

5.5 Correlation of failure analyses to experiment for the 10° off-axis specimens.

Five 10° off-axis specimens, B1– B3, B5 and B6, as described in chapter 4, Fig. 4.4, with dimensions recorded in Table 4.4, were tested under axial tension to failure. During testing, 3-gage rosettes applied to the center of the specimens, as described in chapter 4, were used to record the strain fields. Specimen B1 was instrumented more completely, as also

described in chapter 4. Axial load and the strains were recorded in 0.5 second increments over the 100 second duration of the tests. Loading was in displacement control, with a constant cross-head speed set to achieve approximately 1% strain per minute. Failure was observed closely, from behind a transparent screen.

No damage or failure initiation could be observed before final failure. Failure for these specimens was somewhat less dramatic than the two previous experiments. The laminates remained more intact. Details of typical failed specimens can be seen in Figs. 5.8 and 5.9.

Measured failure loads and stresses are presented in Table 5.13.

TABLE 5.13 Measured 10° off-axis specimen strengths

Specimen	Minimum Area	Failure Load	Failure Stress
	sq. inch	lb.	ksi
B1	0.08374	7217.27	86.19
B2	0.08459	7392.53	87.39
B3	0.08414	7218.49	85.79
B5	0.08470	7435.27	87.78
B6	0.08394	6998.05	83.37
		Ave:	86.05 ksi
		C.O.V.	1.8%

The failure stresses are fairly uniform with a small coefficient of variation, 1.8%. Comparison with predicted last-ply failure is given in Table 5.14.

TABLE 5.14 Experimental and predicted failure loads; off-axis loading.

Method	Failure load	Difference from experiment	Comments
	ksi	%	
Experiment	86.05	n/a	5 specimens, C.O.V= 1.8%
Hart-Smith	143.15	+66.4	
Tsai, temp. and moisture	77.74	-9.7	Hygro-thermal as favored by Tsai.
Tsai, no hygro-thermal	74.27	-13.7	
Tsai, temperature incl.	60.64	-29.5	

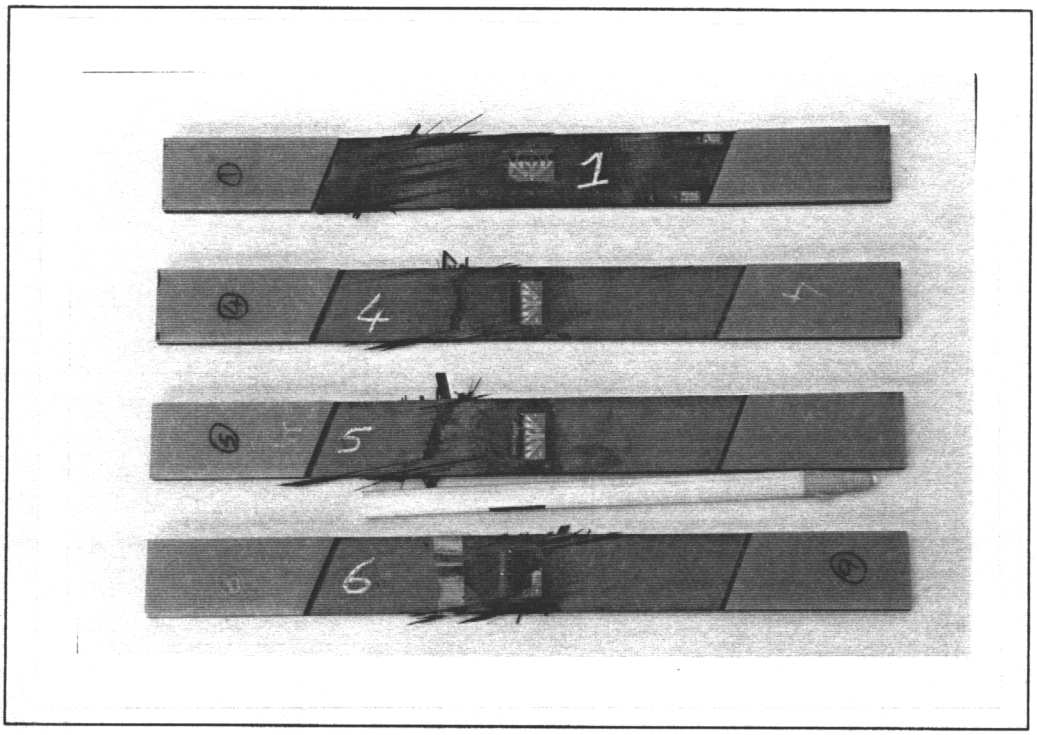

Fig. 5.8 Photograph of typical failed off-axis specimens

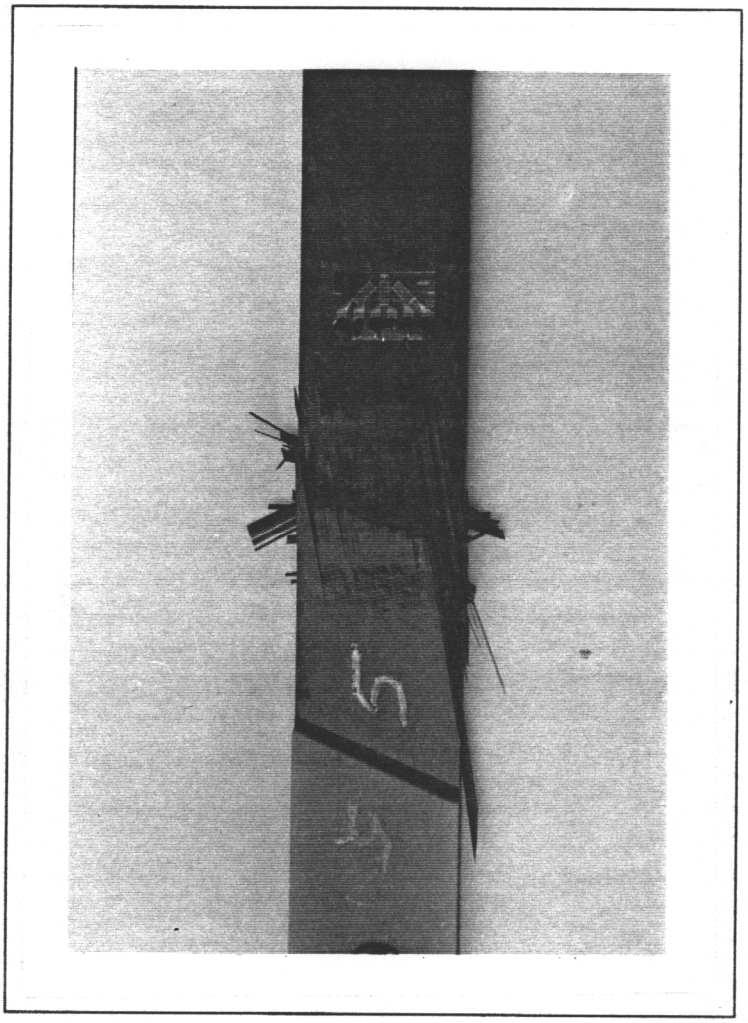

Fig. 5.9 Photograph of failed off-axis specimen B5

Hart-Smith's prediction is now 66.4% too high, while in Tsai's case the prediction is 9.7% lower than experiment. As noted the critical ply for the two criteria are different, with Hart-Smith predicting critical conditions in the 10° ply and Tsai in the -35° ply.

Inspection of the failed specimens revealed that failure occurred at an angle of close to 55° with respect to the load axis in most of the specimens, as shown in Fig. 5.8 and 5.9. This observation tends to support Tsai's prediction that the -35° plies are most critical, as most of the failures seem to be at 90° to the -35° plies. That is, tensile fiber failures in the -35° plies implies a fracture surface roughly normal to the fiber direction, in other words at 55°. If the 10° plies were critical, a fracture surface at 100° may be expected, and no evidence of this can be seen.

Stress-strain information for specimen B1 is shown in Fig. 5.10, plotting σ_x against ε_x, with x referring to the laminate principal axis, here at 10° to the load, as before. Agreement between predictions and experiment in the initial section of the curves is quite close, but not as close as for the on-axis specimens. The experimental curve displays a distinct loss of stiffness towards the higher strains, and at failure the stiffness is almost exactly modeled by Tsai's predictions. Hart-Smith predicts only final failure with no degradation along the way. For Hart-Smith, both the failure load and strain levels are far from those measured. The area of degradation in Fig. 5.10 is displayed in more detail. in Fig. 5.11.

As shown in Fig. 5.11, the match between the Tsai prediction and experiment is very close in the area of degradation. However, the load and strain levels at which degradation is first predicted does not agree well with that measured. The slight mismatch between the measured slope and predicted slope in the initial portion of the stress-strain curves of Fig. 5.10 may influence the agreement detailed in Fig 5.11 to some extent. If the initial slopes were exactly the same, Tsai's curve would not fit the experimental curve quite as well, as it would be rotated slightly with respect to the experimental curve.

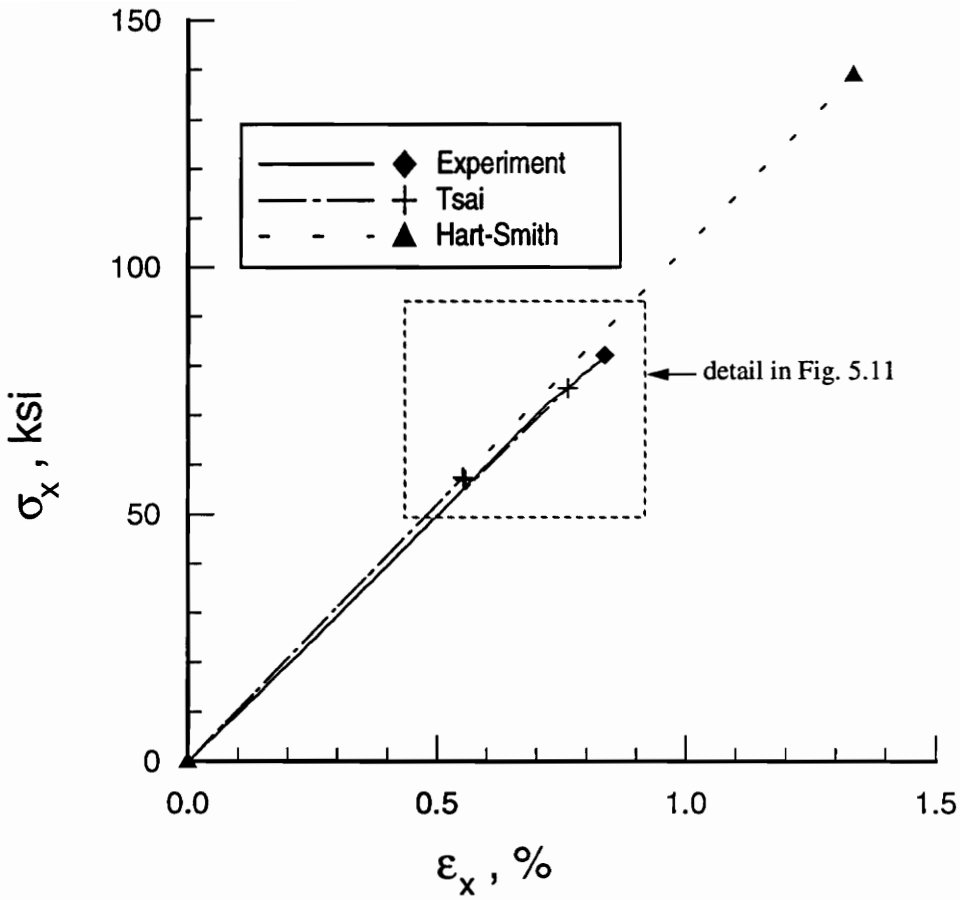

Fig. 5.10 Measured stress, σ_x, vs. strain, ε_x, for specimen B1, with predictions of Tsai and Hart-Smith.

As the degradation phenomenon is matrix dominated, the in-plane shear behavior of the test coupons is of interest. With respect to the X-Y axes, in-plane shear is resisted mainly by fiber tension-compression in the 55° and -35° plies, and by matrix shear in the other plies. With respect to the X-Y directions there is only one set of 55° / -35° plies present in the laminate for every three sets of 10° / 100° plies, meaning matrix effects may dominate under shear loading.

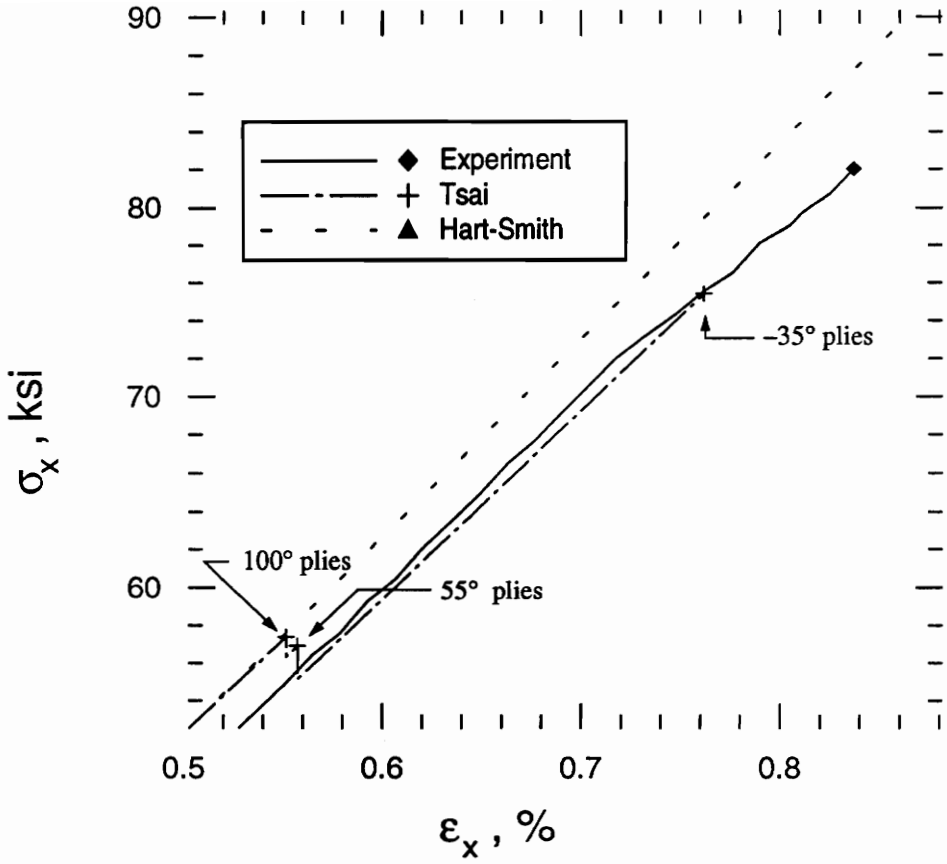

Fig. 5.11 Detail of Fig. 5.10 showing predicted degradation and measured stress-strain path.

The in-plane shear stress-shear strain response for coupon B1 is shown in Fig. 5.12 and compared with predictions. As in Fig 5.10, for axial stress-strain, the Tsai prediction is very close to the predicted stress-strain point at failure, but the initial portion of the curves are not quite parallel. Hart-Smith's prediction is far off the mark, as it was in Fig 5.10. The degradation in stiffness experimentally observed is more marked in Fig 5.12, as opposed to the axial stress strain plots of Figs. 5.10 and 5.11. The softening shear response supports the observation that matrix effects dominate under shear for this laminate.

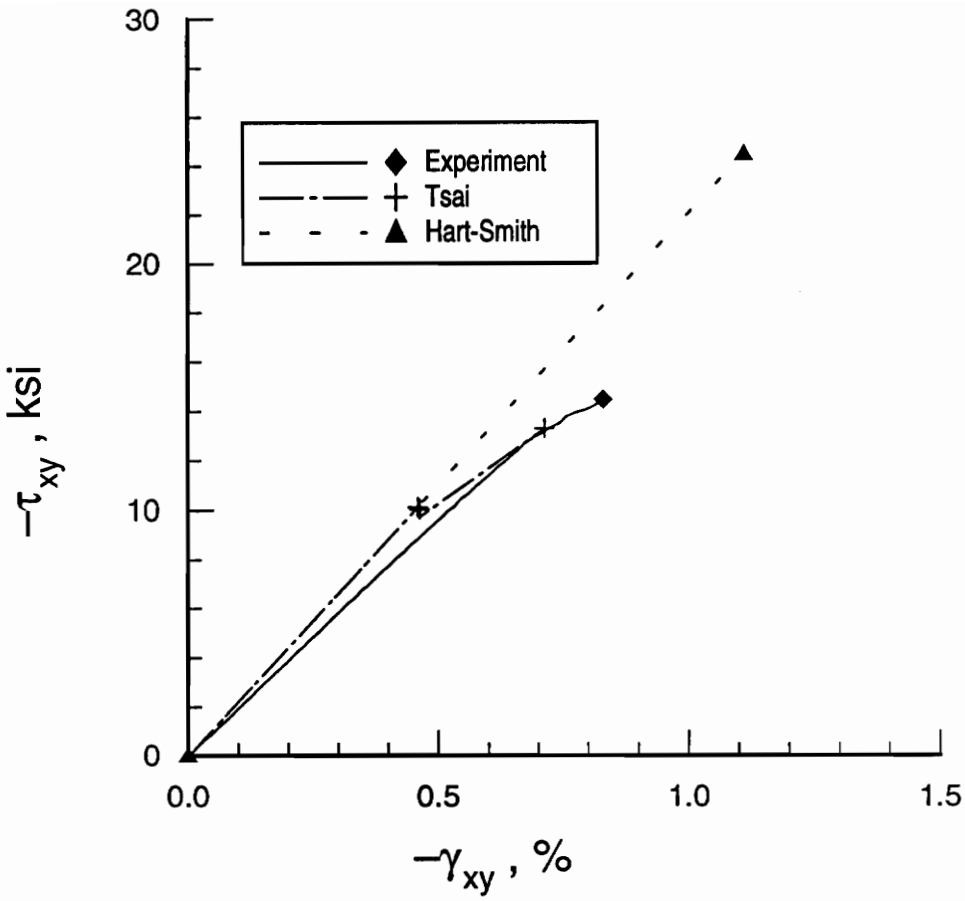

Fig. 5.12 Measured and predicted shear stress-strain curves for specimen B1.

To complete the set, laminate normal strains ε_y and ε_x are plotted in Fig. 5.13 for specimen B1, from experiment and analysis. Here the slopes define the Poisson's ratio of the coupon. The initial slopes are fairly close, but the experimental curve is steeper than predicted by the analysis. The slope of Tsai's curve after degradation is reduced, which does not model the experiment very well.

The stress-strain behavior described for specimen B1 is typical for all the off-axis specimens, and this is consistent with the low coefficient of variation in failure strength found for the off-axis specimens.

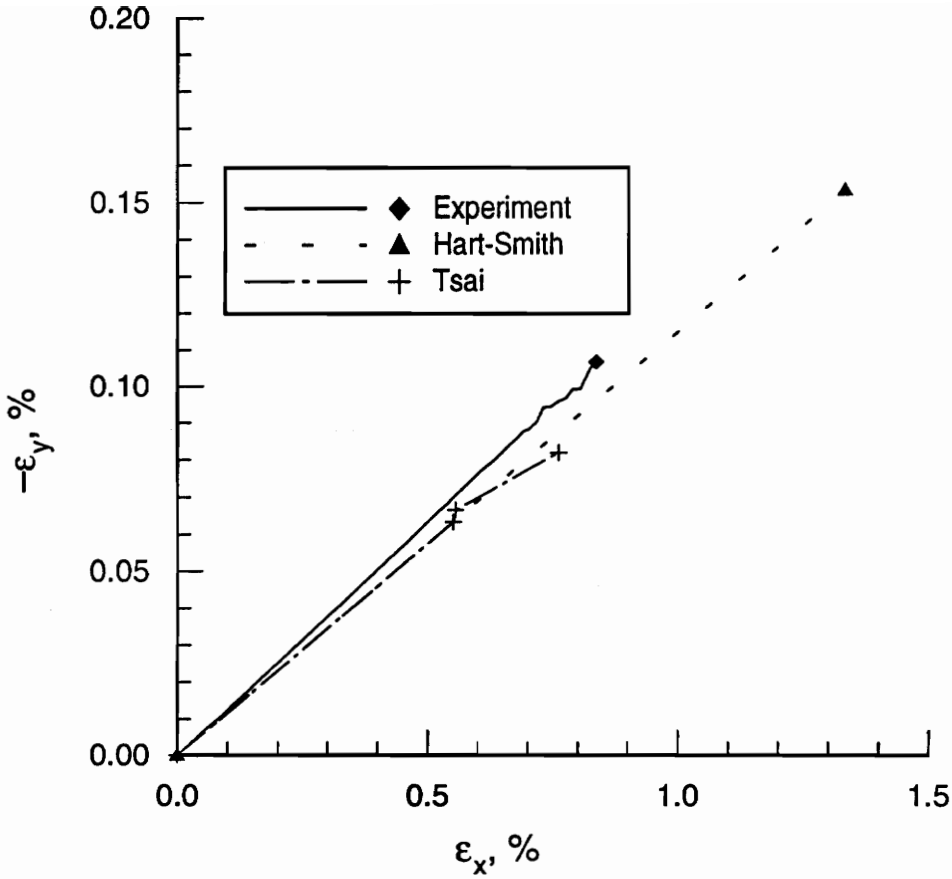

Fig. 5.13 Strain ε_x vs. $-\varepsilon_y$ for specimen B1, with predictions of Tsai and Hart-Smith.

This concludes the description of the experiments. In the next section the experimental results will be discussed more and future work suggested.

5.6 Discussion

Results obtained from experiment were satisfactory throughout. Visual observation of failures, both during testing and of failed coupons, revealed no sign of secondary failure effects such as premature delamination, failures in the grips due to stress concentrations, failure of the laminate-tab bond, or any other experimental problems. Repeatability of the 10° off-axis strength and the on-axis strengths was very good. The coefficient of variation

in the strengths of the 10° off-axis specimens was 1.8%, and for the on-axis specimens it was 2.0%. Test results from only two of the unidirectional specimens were judged unsatisfactory. The coefficient of variation in the strengths of the remaining unidirectional specimens was a very acceptable 3.1%.

Particularly worthy of note is the performance of the oblique tabs used for the off-axis specimens. The strain field measured, (see Fig. 5.7), is extremely uniform, with no evidence of axial-shear coupling effects. These tabs seem to open the door to a whole range of experiments that have been either avoided in the past, or required extensive and expensive preparation. It should be noted, however, that for the laminates used here, the extension-shear coupling while significant, was not very large. Sun and Chung conducted experiments on 20° off-axis coupons made from unidirectional material, for which the $-\frac{\bar{A}_{16}^{-1}}{\bar{A}_{11}^{-1}}$ ratio was equal to 1.8, with a corresponding tab angle, ψ, of 29° [23]. For the specimens tested here, $-\frac{\bar{A}_{16}^{-1}}{\bar{A}_{11}^{-1}}$ was equal to 0.5, with a corresponding tab angle of $\psi = 63.5°$. Sun and Chung nevertheless obtained strain fields similar to those measured here.

An area of experiment that may require more attention may be the loading rate. Observations during the present experiments were made visually, and the experiments proceeded rather quickly. It may be worthwhile to monitor the experiment while it is being conducted more slowly. In addition, more sophisticated equipment may be used to observe the failure, a high-speed camera comes to mind. Using x-ray equipment, or other nondestructive inspection techniques to detect matrix cracking, if any, may be useful.

As noted in section 5.2 the on-axis specimen tests produced results very close to both the predictions of Tsai and Hart-Smith. Hart-Smith's criterion models fiber failure only, and it is interesting that in this undoubtedly fiber dominated case his prediction is indeed closest to experiment, at 1.7% higher, as compared to Tsai's 8.4% lower prediction. The degradation observed in these tests is, however, not modeled by Hart-Smith's criterion, and it may be interesting to investigate this effect. By chance this was done on one specimen that was inadvertently loaded to 90% of the average tensile failure load, unloaded and reloaded in tension to failure. This specimen failed at 5% less than the average failure load, which, while not enough difference to state that degradation is significant, may provide a clue as

to how this effect may be investigated. It would be interesting to conduct a compression test of a specimen that was previously loaded to 90% of its tensile strength. Compression strength is likely to be more sensitive to laminate degradation than tensile strength.

For the 10° off-axis case the failure predictions of Tsai and Hart-Smith show a large difference. The state of strain differs from the on-axis case, mainly by the presence of in-plane shear. Since the two criteria treat this effect very differently, this characteristic is most likely to be the reason for the big difference. Experimental results show that Tsai's predictions are much closer to the experiment, both in the prediction of stress-strain paths, and in the failure load. Tsai's progressive damage model underestimates the experimental failure load by 9.7% for the 10° off-axis specimens and 8.4% for the on-axis specimens. Consistently underestimating the failure load by less than 10% is a feature very reassuring to designers.

The degradation modeled by Tsai's criterion and not by Hart-Smith's seems to lie at the heart of the differences observed. Hart-Smith argues that for laminates loaded in in-plane shear the required plies at ±45° to the axes of the shear will support the laminate sufficiently so that the resulting shear deformation will be small enough that neither the "soft" matrix or the "stiff" 0°/90° fibers will be unduly strained. The present experimental laminate meets the requirement of 12.5% fibers in each of the 45° and –45° directions to the shear axes. However, a measurable loss of axial and particularly shear modulus is observed, that cannot be attributed to the brittle fibers, disproving the assertion that the matrix will not be affected.

However, before rejecting Hart-Smith's treatment of in-plane shear, attention should focus on the coupon used. Scaling effects are known to be present in angle ply composite coupons [24]. In particular, the coupons used here have very few fibers running from tab to tab. This implies that the brittle matrix is relied upon to transfer load from the fibers terminating at the free edges to adjacent fibers. One way in which this free edge effect may be investigated is the use of wider specimens, i.e., specimens with a lower aspect ratio. Such specimens will have more fibers supported in both tabbed ends.

Given the success obtained here with oblique tabs for overcoming the scourge of extension-shear coupling in off-axis test coupons, tests on low aspect ratio coupons should be feasible.

Should lower aspect ratio coupons reveal failure stresses closer to Hart-Smith's predictions, and reveal less softening attributable to the matrix, the failure loads here may be attributed to matrix effects peculiar to the test coupon, and the present results rejected as unrepresentative of the conditions imposed by Hart-Smith; i.e., fiber dominated laminates. If similar behavior to that found here is observed in wider coupons, the conclusion that Hart-Smith's treatment of in-plane shear is incorrect may safely be drawn.

Another aspect of present work worthy of further investigation is the mismatch observed in the predicted and measured stiffnesses of off-axis coupons. These differences, though small, tend to obscure the true effectiveness of Tsai's modeling of degradation, as noted before in the discussion on the match of experiment and theory in Figs. 5.10 and 5.11. It may be advantageous to experimentally characterize the material more completely, particularly the matrix dominated moduli E_y and G_{12}.

Whatever present and future investigations of the mechanics of failure reveal, the objective of using optimization to design a test coupon and load type to sharpen the difference between two theories have certainly been met. The fact that uncertainty on the exact reason for the differences exist does not detract from this. The object was specifically to find areas of disagreement, and that implies that the following step would be consideration of how to reconcile or explain the differences.

The optimization process was successful in revealing two areas of large difference in failure load prediction for the two criteria. The first area was the predicted failure load for compression-compression loading, and the second was combined tension and shear loading. The largest differences were predicted in the first case, and this area of compression-compression loading, should also be investigated experimentally.

Chapter 6 : Summary and Conclusions

In this study the use of optimization in designing experiments to discriminate between competing models of the same phenomenon was described. The phenomenon considered was the failure of laminated filamentary composite materials under in-plane loads. The models compared were the failure criterion of Tsai including both degradation and progressive failure, and the failure criterion of Hart-Smith. Experiments were performed to examine experimental conditions found by the optimization process. In this chapter the present study is summarized, and conclusions drawn.

6.1 Summary

Optimization techniques were used to design laminate-load combinations that optimize an objective function, F, with F given by the ratio of predicted failure load for the criterion of Hart-Smith to the predicted failure load for the criterion of Tsai. Sixteen-ply, balanced and symmetric laminates with at least one ply in each of the 0°, 90°, 45°, and -45° fiber directions were considered. Nominal material properties were used in the optimization phase, and hygro-thermal effects were ignored.

First, general in-plane load and laminate combinations were optimized. A genetic algorithm was used in the optimization. The minimum objective function found was as F = 0.4008, for the laminate $[\pm 45 / 90_2 / 0_4]_s$, and base load vector, $N_x : N_y : N_{xy}$ of -0.796 : -0.605 : 0.00. The maximum objective function was F = 1.890, for the laminate $[\pm 45 / 90 / 0_5]_s$, and base load vector, $N_x : N_y : N_{xy}$, of -0.438 : 0.787 : 0.434.

Next laminate-load combinations suitable for experiments were designed. The maximum value of the objective function under general loading occurred for a case of combined axial and in-plane shear loads. This loading was approximated by uniaxial loading of off-axis specimens. Laminate designs for uniaxial tension were evaluated for several off-axis angles. The maximum value of F was found for the laminate $[\pm 45 / 90 / 0_5]_s$, and occurred at 22° off-axis angle. This laminate had an objective function value of F = 1.832, which was close to the theoretical maximum of F = 1.890.

For practical reasons the laminate $[0_3 / 90_3 / \pm 45]_s$, with F = 1.579, loaded at 10° off-axis angle was selected for testing. An approximate delamination analysis was used to distribute the plies through the thickness in order to minimize the interlaminar pealing stress at free edges. Consequently, the sixteen-ply laminate selected for testing had the stacking sequence of $[0 / 90 / 45 / 0 / 90 / -45 / 90 / 0]_s$. In addition to 10° off-axis testing, on-axis tests were performed on the same laminate, as a check of the criteria's performance under simple loading.

The material used in experiments was BASF G30-500 / 5208. Material properties were found from supplier data sheets, literature, and experiment. Eight, eight-ply unidirectional specimens were tested in uniaxial tension to failure to determine the fiber-direction

strength, X, modulus, E_1, and major Poisson's ratio, ν_{12}. The test result for E_1 had a coefficient of variation of 2.5%, while both X and ν_{12} had the coefficient of variation of 3.1%.

The on-axis laminate was reanalyzed using material properties for the BASF material and hygro-thermal effects where reasonable. Eight on-axis specimens were tested in uniaxial tension to failure. Stress and strain information was also recorded. The specimens consistently failed in the gage section. The coefficient of variation in measured strength was 2.0%. Hart-Smith's strength prediction was 1.7% higher than measured, and Tsai's prediction including hygro-thermal effects was 8.42% lower. Some decrease in fiber direction modulus could be observed in the experiments, similar to that modeled by Tsai. In general no significant difference between the two failure criteria could be established from on-axis tests.

For off-axis tests the failure load predictions were repeated using the relevant material properties and hygro-thermal effects, as described above. Five off-axis specimens were tested in tension to failure, and stress-strain information was recorded. The specimens consistently failed in the gage section.

Oblique bonded tabs as described by Sun and Chung, [23], were used to accommodate the axial-shear coupling effect in the off-axis specimens. Strain gages close to the tabs and gages in the gage section reported virtually indistinguishable strains, indicating that a homogeneous in-plane strain field was achieved.

Off-axis specimen failure loads had a coefficient of variation of 1.8%. The predicted failure load of Hart-Smith was 66.4% higher than experiment and Tsai's prediction was 9.7% lower than experiment. Tsai's predicted stress-strain response modeled the observed degradation quite well, while Hart-Smith's theory ignored degradation.

This concludes the summary of the work. The next section lists conclusions drawn from the study.

6.2 Conclusions

To start with the objectives of the study stated in chapter 1 are repeated:

- First, the study focused on the use of optimization techniques to design experiments that differentiate between competing models of the same phenomenon.
- Second, this idea was applied to failure criteria for filamentary composite materials with the objective of examining their relative merit when compared to experiment.

The following conclusions can be drawn from the material presented in this work:

- Optimization techniques were successfully used in identifying two areas of disagreement between the failure predictions of the Tsai and Hart-Smith failure criteria; namely, the prediction of biaxial compression failure loads, and the prediction of combined axial tension and in-plane shear failure load.
- In addition to using optimization to find areas of general disagreement between the two failure criteria, optimization was instrumental in designing specimens for specific test conditions.
- The differences in failure load prediction between the two criteria are thought to be related to the different treatment of in-plane shear.
- The experimental program was very successful, with excellent repeatability of measured failure loads, material properties, and stress-strain response.
- Oblique bonded tabs are an invaluable tool for achieving uniform strain fields when testing off-axis specimens in tension.
- Tsai's failure criterion predicted loads that were consistently slightly below the experimental failure load for both on-axis and off-axis specimens, while Hart-Smith's criterion was accurate in predicting on-axis failure load, but overpredicted off-axis failure load by a large amount.
- Both fiber direction modulus and shear modulus degradation was observed in experiments.

An open question regarding the length to width ratio of the 10° off-axis specimen remains. Since the specimens used here had a length to width ratio in the gage section of 5.5, very few fibers ran from tab to tab. This implies a free edge effect is present in which fibers terminating at the longitudinal free edge must transfer their load through the brittle matrix to adjacent fibers. This free edge effect may result in a matrix dominated ultimate failure, which is not predictable by Hart-Smith's criterion. Thus, off-axis tests on wider specimens are needed to investigate this free edge effect.

References

1 Rowlands, R. E., "Strength (Failure) Theories and their Experimental Correlation," in Handbook of Composites; vol.3: "*Failure Mechanics of Composites*," Sih, G. C., and Skurda, A. M. (eds.), Elsevier Science Publishers, Amsterdam, 1985.

2 Haftka, R. T, "*Optimization and Experiments*," private communication.

3 Beck, J. V., and Arnold, K. J., "*Parameter Estimation*," John Wiley and Sons, Inc., New York, 1977.

4 Haftka, R. T., and Kao, P., "The Use of Optimization for Sharpening Differences Between Models," in *Recent Developments in Composite Materials Structures*, ASME Winter Annual Meeting, 1990.

5 Tsai, S. W., "*Theory of Composites Design*", Think Composites, Dayton Ohio, 1992.

6 Hart-Smith, J. L., "A New Approach to Composite Laminate Strength Prediction," Douglas Paper 8366, presented to MIL-HDBK-17 Committee Meeting, Palm Beach, Florida, October 3-5, 1989; *Proceedings of the 8th DoD/NASA/FAA Conference on Fibrous composites in Structural Design*, Norfolk, Virginia, November 28-30, 1989, NASA CP-3087, Part 2, pp. 663-693.

7 Hart-Smith, J. L., "A Strain-Based Maximum Shear-Stress Failure Criterion for Fibrous Composites," Douglas Paper 8376, presented to *31st Annual AIAA/ASME/ ASCE/AHS/ASC Structures, Structural Dynamics and Materials Conference*, Long Beach California, April 2-4, 1990.

8 Jones, R. M., "*Mechanics of Composite Materials*," Hemisphere Publishing Corporation, New York, 1975.

9 Hart-Smith, J. L., "Composite Laminate Strength Prediction Demistified," Douglas Paper 8430, presented to *11th European SAMPE Conference*, Basel Switzerland, May 29-31, 1990.

10 Azzi, V. D., and Tsai, S. W., "Anisotropic Strength of Composites," *Experimental Mechanics*, 5(9), 1965, 283-288.

11 Hoffman, O., "The Brittle Strength of Orthotropic Materials," *Journal of Composite Materials*, 1, 1967, 200-206.

12 Gol'denblat, I. I., and Kopnov, V. A., "Strength of Glass-Reinforced Plastics in the Complex Stress State," *Mechanica Polimerov*, Vol. 1, 1965, p. 70; English translation: *Polymer Mechanics*, Vol. 1 , Faraday Press, 1966, p 54.

13 Tsai, S. W., and Wu, E. M., "A General Theory of Strength for Anisotropic Materials," *Journal of Composite Materials*, January 1971, pp. 58-80.

14 Tsai,S. W., "*Composites Design*," 4th edition, Think Composites, Dayton, Ohio, 1988.

15 Hart-Smith, J. L., "A Scientific Approach to Composite Laminate Strength Prediction," Douglas Paper 8467, *Proceedings of the 10th ASTM Symposium on Composite Materials: Testing and Design*, San Francisco, California, April 24-25, 1990, STP 1120.

16 Drazal, L. T., Rich, M. J., Koening, M. F., and Loyd, P. F., "Adhesion of Graphite Fibers to Epoxy Matrixes; II The Effect of Fiber Finish," *Journal of Adhesion*, Vol. 16, 1983, pp. 133-152.

17 Hart-Smith, J. L., 'Backing out Equivalent Unidirectional Lamina Strengths from Tests on Cross-Plied Laminates," Douglas Paper MDC 91K0078; *Proceedings of the 37th International SAMPE Symposium and Exhibition*, Anaheim, California, March 9-12, 1992.

18 Tsai, S.W., and Hahn, "*Introduction to composite materials*," Technomic Publishing Company, Inc., Lancaster, Pennsylvania.

19 Pagano, N. J., and Pipes, R. B., "Some Observations on the Interlaminar Strength of Composite Laminates," *International Journal of mechanical Sciences*, Vol. 15, 1973, pp. 679-688.

20 Goldberg, D. E., "*Genetic Algorithms in Search, Optimization, and Machine Learning*," Addison-Wesley Publishing Co. Inc., Reading, Massachusetts, 1989.

21 Haftka, R. T., and Gürdal, Z., "*Elements of Structural Optimization*," 3rd edition, Kluwer Academic Publishers, Dordrecht, the Netherlands, 1992.

22 Le Riche, R., and Haftka, R. T., "Optimization of laminate Stacking Sequence for Buckling Load Maximization by Genetic Algorithm," *Proceedings of the AIAA/ASME/ASCE/AHS/ASC 33th Structures, Structural Dynamics, and Materials Conference*, Dallas, Texas, April, 1992.

23 Sun, C. T., and Chung, I., "An Oblique End Tab Design for Testing Off-Axis Composite Specimens," in *Recent Developments in Composite Materials Structures*, ASME Winter Annual Meeting, Aerospace Division, AD v 19, 1990, pp. 7-11.

24 Kellas, S. and Morton, J., "Strength Scaling in Fiber Composites," *NASA Contractor Report*, CR–4335, 1990

Vita

The author was born on December 19, 1966 in Pretoria, South Africa. A few years later he started an academic career lasting to this day, with enrollment at the Gelofte Primary School in Pinetown, Natal. After attending various other schools he graduated from the Overkruin High School in Pretoria in December 1984. After enduring two years in the South African Air Force as a conscript, he enrolled at the University of Pretoria, and graduated Cum Laude with a Bachelors Degree in Mechanical Engineering in December 1990. The next five months was spent in the Netherlands at the Technical University of Delft. A Fulbright Scholarship made graduate study in the US possible, and in August 1991 he enrolled for a Masters Degree in Aerospace Engineering at Virginia Polytechnic Institute and State University.